Unclassified
SECURITY CLASSIFICATION OF THIS PAGE

AD-A212 921

(2)

REPORT DOCUMENTATION PAGE

1a REPORT SECURITY CLASSIFICATION: Unclassified

1b RESTRICTIVE MARKINGS

2a SECURITY CLASSIFICATION AUTHORITY

3 DISTRIBUTION/AVAILABILITY OF REPORT: Approved for public release; Unlimited Distribution

2b DECLASSIFICATION/DOWNGRADING SCHEDULE

4 PERFORMING ORGANIZATION REPORT NUMBER(S)

5 MONITORING ORGANIZATION REPORT NUMBER(S): AFOSR-TR- 89-1232

6a NAME OF PERFORMING ORGANIZATION: United Technologies Optical Systems

6b OFFICE SYMBOL (If applicable)

7a NAME OF MONITORING ORGANIZATION: AFOSR/NP

6c ADDRESS (City, State, and ZIP Code): United Technologies Optical Systems, P.O. Box 109660, West Palm Beach, FL 33410

7b ADDRESS (City, State, and ZIP Code): Bldg 410, Bolling AFB DC 20332-6448

8a NAME OF FUNDING/SPONSORING ORGANIZATION: Air Force Office of Scientific Research

8b OFFICE SYMBOL (If applicable): NP

9 PROCUREMENT INSTRUMENT IDENTIFICATION NUMBER: F49620-88-C-0031

8c ADDRESS (City, State, and ZIP Code): Building 410, Bolling, AFB, DC 20332-6448

10 SOURCE OF FUNDING NUMBERS

PROGRAM ELEMENT NO.	PROJECT NO.	TASK NO.	WORK UNIT ACCESSION NO
61102F	2301	A4	

11 TITLE (Include Security Classification)

"Experimental and Theoretical Study of CO_2 Staggered Hollow-Bore Array Lasers"

12 PERSONAL AUTHOR(S): D. Park, R.A. Hart, and L.A. Newman

13a TYPE OF REPORT	13b TIME COVERED	14 DATE OF REPORT (Year, Month, Day)	15 PAGE COUNT
Final Report	FROM 8/1/88 TO 6/30/89	August 20, 1989	58

16 SUPPLEMENTARY NOTATION

17 COSATI CODES			18 SUBJECT TERMS (Continue on reverse if necessary and identify by block number)
FIELD	GROUP	SUB-GROUP	
	20.06		Arrays, Laser, Staggered, Waveguide, Optical, Hollow-Bore.

19 ABSTRACT (Continue on reverse if necessary and identify by block number)

Experimental and theoretical investigation of CO_2 staggered hollow-bore (SHB) arrayswere conducted with the main objective of gaining a better understanding of the device. By focussing on the effects of a mirror tilt on the output power, the near field and pairwise far field patterns, we have deduced that the effective cavity length variations, manifested primarily through mode mismatch loss, are responsible for many of the observed features of phase-locked SHB arrays. We also found that by making one of the elements very lossy, we can effectively shut down the entire array, which could have a potential application as a novel amplitude modulation technique.

89 9 27 031

20 DISTRIBUTION/AVAILABILITY OF ABSTRACT: ☐ UNCLASSIFIED/UNLIMITED ☒ SAME AS RPT ☐ DTIC USERS

21 ABSTRACT SECURITY CLASSIFICATION: Unclassified

22a NAME OF RESPONSIBLE INDIVIDUAL	22b TELEPHONE (Include Area Code)	22c OFFICE SYMBOL
Howard K. Schlossberg	202-767-4906	NP

DD FORM 1473, 84 MAR — 83 APR edition may be used until exhausted. All other editions are obsolete.

SECURITY CLASSIFICATION OF THIS PAGE: Unclassified

R89-984002

EXPERIMENTAL AND THEORETICAL STUDY OF CO_2 STAGGERED HOLLOW-BORE ARRAY LASERS

Prepared by
D. Park
R.A. Hart
L.A. Newman

Final Report
August, 1989

Sponsored by the Department of the Air Force
Under Contract F49620-88-C-0031

UNITED
TECHNOLOGIES
OPTICAL SYSTEMS
West Palm Beach, Florida 33410-9660

R89-984002

EXPERIMENTAL AND THEORETICAL STUDY OF CO_2 STAGGERED HOLLOW-BORE ARRAY LASERS

Prepared by
D. Park
R.A. Hart
L.A. Newman

Final Report
August, 1989

Sponsored by the Department of the Air Force
Under Contract F49620-88-C-0031

UNITED
TECHNOLOGIES
OPTICAL SYSTEMS
West Palm Beach, Florida 33410-9660

Experimental and Theoretical Study of CO_2 Staggered Hollow-Bore Array Lasers

TABLE OF CONTENTS

LIST OF FIGURES

LIST OF TABLES

Relation Information

Publications:

Submission of manuscript is planned for Applied Physics Letters and IEEE Journal of Quantum Electronics.

Patent Disclosure:

A patent disclosure entitled "A Modulation Technique for Staggered Hollow-Bore Array Lasers" has been written.

List of Professional Personnel Associated with the Research:

Dr. Dongwook Park
Mr. Richard A. Hart
Dr. Leon A. Newman

Experimental and Theoretical Study of CO_2 Staggered Hollow-Bore Array Lasers

1.0 INTRODUCTION

From June 1984 to September 1987, United Technologies Research Center (UTRC), under the sponsorship of the Air Force Office of Scientific Research Contract Nos. F494602-C-0062 and F49620-85-C0109, conducted research to explore unique ridge waveguide techniques for phase-locking coupled waveguide lasers. The motivation for investigating coupled waveguide laser arrays was to scale their output power according to the number of elements in the array while maintaining single frequency operation. Several designs were considered and tested, among which the staggered hollow-bore (SHB) arrays proved to be most desirable in terms of the loss, mode discrimination, and single frequency operation [1-5]. There has been, however, a lack of general understanding of the SHB arrays; it is necessary to gain a better insight into how the device works and what parameters are important in order to improve SHB array's performance.

The objective of this program is to study coupled high power CO_2 waveguide laser arrays, staggered hollow-bore arrays to be exact, both experimentally and theoretically so that ultimately a means of obtaining greater output power and a more uniform array pattern may be devised. However, as the priority of the program is on understanding the array's behavior, no modifications are made to the waveguide strcuture in an attempt to improve the laser's performance.

Section 2 describes the experimental effort which had a two-tiered structure: one, a parametric study of larger arrays, and two, a close look at simpler structures to lend supporting - or refuting - evidences to those premises based on the previous results. It was found that the differences in effective cavity lengths of an array can lead to a tapered intensity distribution across the array and also a power loss vis a vis with the uniform cavity length case. In a related finding, a large loss in just one element of the array turned out to significantly affect the entire array. Section 3 describes the theoretical portion of the research, which concentrated on trying to explain the observed experimental phenomena; it includes first-order theories on the primary loss mechanisms, especially the mode mismatch loss mechanism, and formuations on how to solve for the supermodes and locking behaviors. Section 4 assesses the findings of this research program and points out some possible directions for future work in the area of phase-locked arrays.

1.1 Background

The basic concept behind staggered hollow-bore arrays lies in that

because of the alternating positions of the two sets of dividing walls [see Figure 1-1], the array would naturally favor the EH_{21} waveguide mode in each channel, wherein the two lobes of the field would differ in phase by 180° [see Refs. [3] and [5] for a more detailed description]. In reality, however, the two lobes are not out of phase by 180° and, more importantly, the array intensity distribution has been observed to be highly nonuniform in some cases [3]. Clearly, scaling of the output power - according to the number of elements in the array - would not be possible, were this pattern of tapered distribution to hold for an arbitrary number of elements. These "imperfections" provided clues which, in part, helped shape the direction of the research program.

Many of the concepts and experimental features included in this report are discussed in a rather concise manner as they have already been expounded upon in previous reports [1-3]. Interested readers are advised to refer to them for more details.

1.2 Program Summary

Chief accomplishments of the program have been establishing a connection between the effective cavity length variations and the output power, and demonstrating the potential for modulating an entire array by controlling the loss in just one of the elements in the array. Mode mismatch loss was singled out as the likely mechanism responsible for the former. In the process, a novel technique employing pairwise far field pattern measurements was used to estimate the phase profile of the field in the array. The following is a list of key results.

1) Establishment of a connection between the effective cavity length variations and the output power.

2) Demonstration of a concept for a potential amplitude modulator which requires modulation of the field in just one or two elements of the array.

3) Detailed analysis of the mode mismatch loss mechanism; especially, examination of its dependence on the amplitude and phase imbalance between the fields in adjacent guides. Results used to explain the output power and array pattern behavior.

4) Estimation of the phase profile of the array based on pairwise far field patterns. The profile linked to a spread in effective cavity lengths.

5) Measurements of the far and near field patterns of two-, eight-, and ten-element arrays.

6) Parametric study of the output power: its dependence on the input power and pressure for the two- and ten-element arrays.

7) Observation of the "in-phase" and "out-of-phase" modes during phase-locked operation of the two-element array (Not of the SHB

geometry).

8) Observations of very uneven discharge distributions in an uncoupled ten-element array

Figure 1-1 Schematic Representation of a Staggered Hollow-Bore Array

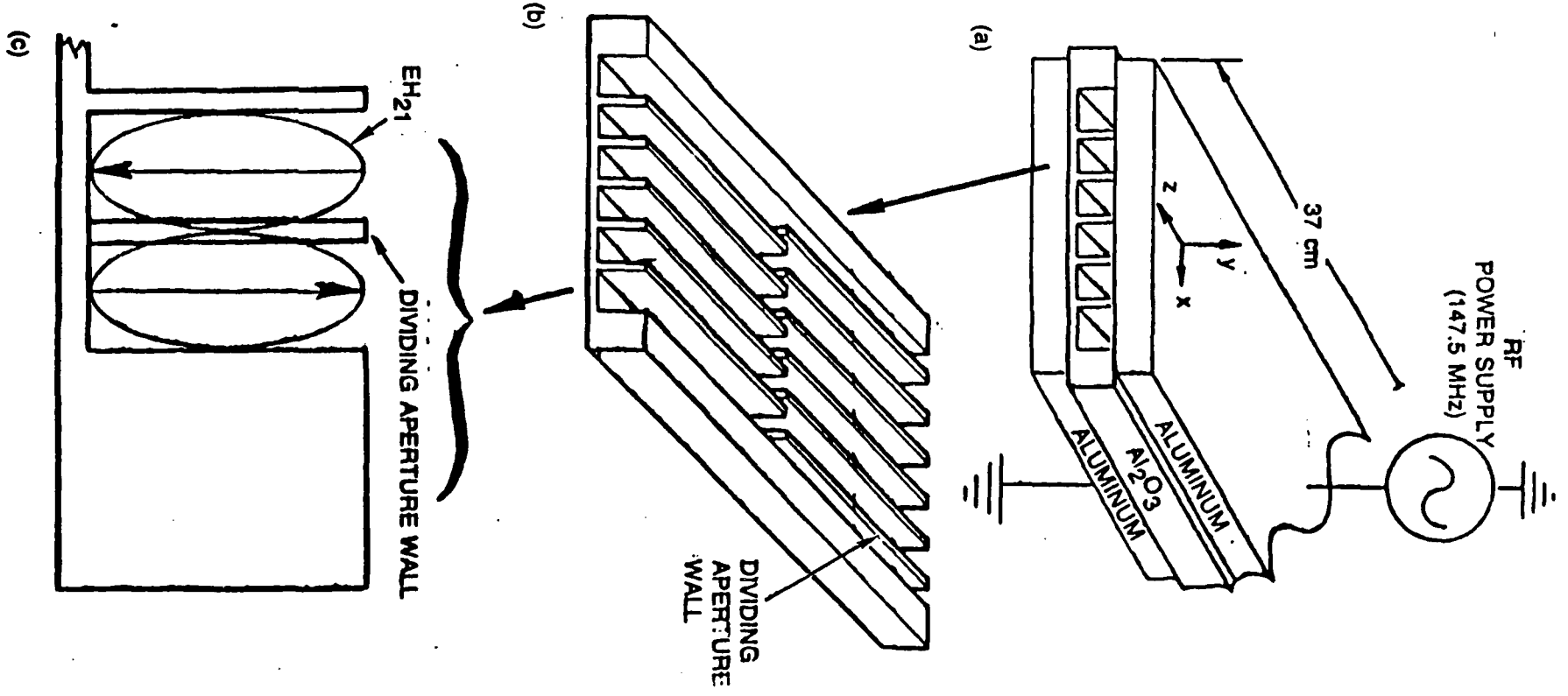

(a) Schematic representation of a staggered array laser with RF excitation.
(b) Staggered ridge hollow-bore alumina waveguide slab.
(c) End view of one channel. The dividing aperture wall begins at the halfway point along the length of the slab.

2.0 DESCRIPTION OF THE EXPERIMENTAL EFFORT

2.1 Experimental Setup

Figure 2-1 is a schematic illustration of the 37 cm waveguide laser array test bed used for this program. Its features have been well documented in [3]. It is, nevertheless, worthwhile to point out the importance of the PZT-actuated mirrors since these ZnSe mirrors produce a change in the cavity lengths: whereas the PZT on the total [maximum] reflecting mirror introduces a uniform change across the array, the PZT mounted on the output coupler mirror introduces a linear variation. Also, it should be mentioned that only the SHB arrays with rectangular channels - as opposed to round channels - were used throughout the experiments.

Figure 2-2 is a schematic of the experimental setup as laid out on the optical bench. Basically five methods were employed to diagnose the laser output: output power measurement; spectral analysis; far field intensity pattern; near field intensity pattern; and thermal imaging plate patterns. The output power measurement was done with a removable power meter while the spectral content of the output was examined with an AuGe detector in conjunction with a spectrum analyzer. A visual inspection of the beam was made with the help of a thermal plate at various locations, e.g., at the beam dump and in front of the pyro detector. Finally, the far field and the near field intensity scans - one-dimensional - were obtained at a common plane by directing the beam through spherical mirrors of different focal lengths and then through a common scanner to the pyro detector, which was then connected to a scope. In order to minize the error associated with estimation of the position of near field plane, a transmission grating and a flashlight were placed at the site of the laser and the location with the clearest image of the grating was marked off as the detection plane for the near field image.

Figure 2-1 37 cm Waveguide Laser Array Testbed

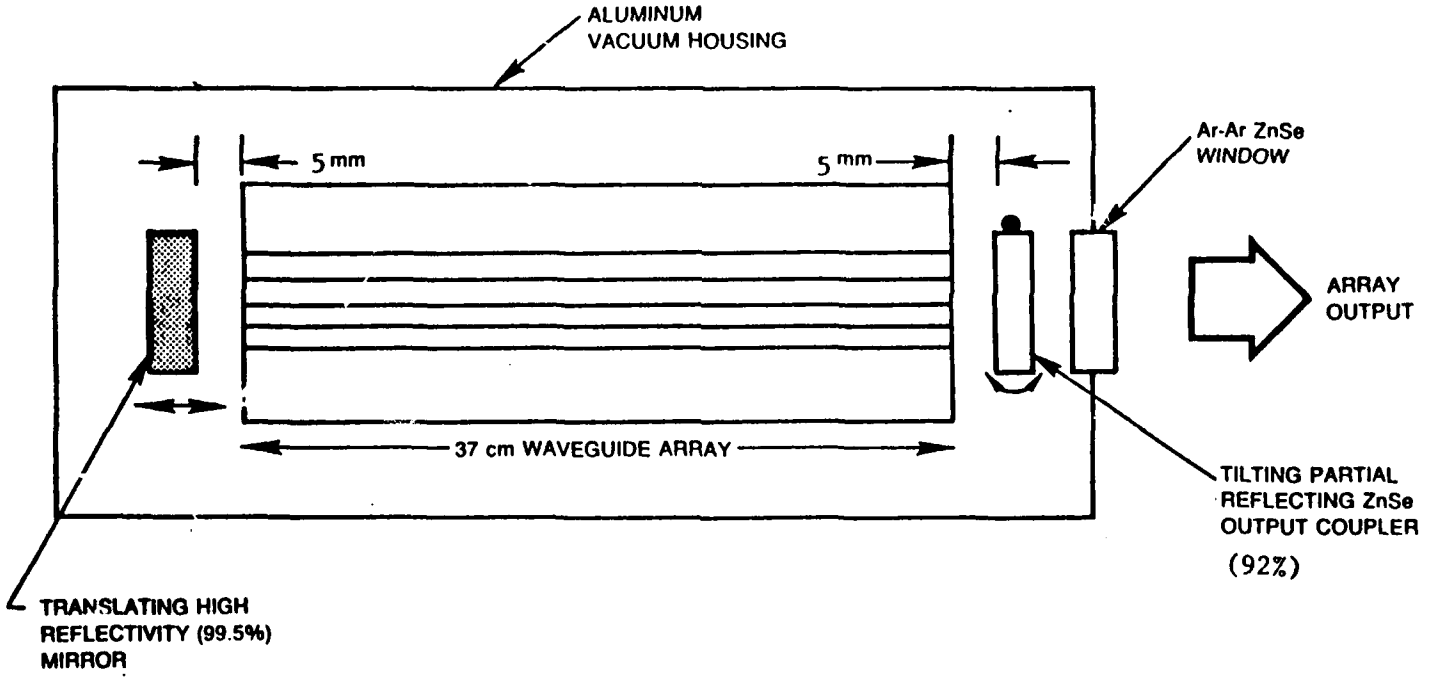

Figure 2-2 Schematic of the Actual Optical Bench Setup

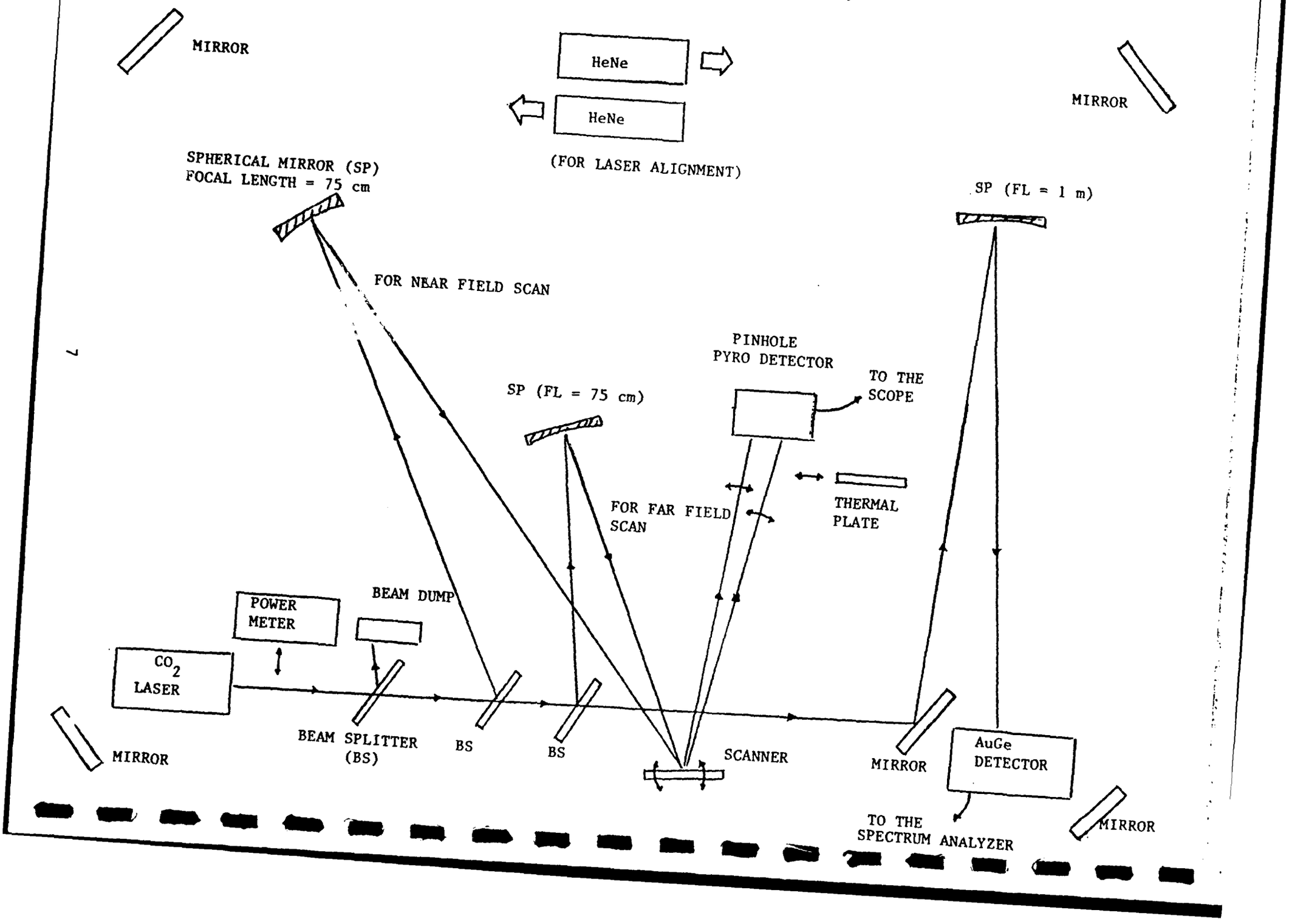

2.2 Experimental Results for an Eight-Element SHB Array

In this segment of the experiment, the key quantities of interest to us were: the shapes of the field patterns - both near and far fields; the output power level; and the phase relationship among the different lobes in the array. Measurements of these quantities would subsequently be used to examine the behavior of SHB array.

The output coupler end of the array had five channels, with the middle three channels having dimensions of 105 mils x 90 mils each and the two end channels measuring 50 mils x 90 mils each. The dividing aperture walls were approximately 6 mils thick each.

A couple of remarks can be made regarding the near field intensity scan, i.e., the horizontal profile of the optical beam intensity at the output plane of the waveguide array. One, as can be seen from Figure 2-3, the intensity tapers off away from the center of the array, rather than being uniform. This point is of great practical importance since it prevents an efficient scaling of power in going from a single-channel structure to a multi-channel array structure. Two, the field distribution within each channel is slightly asymmetric, indicating that the field does not quite conform to the EH_{21} waveguide mode [although it is no doubt the predominant component]. Finally, the field does not have a deep valley at the center of each channel that it does at the dividing wall positions.

A far field scan can give an indication of the relative phases of the lobes in the array [Loosely speaking, each "lobe" refers to a field distribution that is marked by a clear minimum on each side]: a double-lobed, symmetric far field intensity scan would imply that the phase of the lobes differ from those of their adjacent lobes by 180°, whereas an asymmetric pattern favoring one side over the other would be a proof to the contrary. The two asymmetric lobes in Figure 2-4 show clearly that the assumption of the phase of the lobes alternating in sign from one element to the next is not quite true. That the two lobes are nearly equal does, however, indicate that the main component in the optical field in each of the guides is indeed the EH_{21} mode. [A visual inspection of the thermal plate images confirms that the it is ineeed the EH_{21} mode rather than EH_{22} mode] Intuitively, we would suspect that the inevitable differences in the cavity lengths of the array would forbid the phases to differ by exactly 180° even if the EH_{21} mode were the only component. This, and a suspicion that cavity length differences may also manifest themselves in the form of a decreased output power led us to the set of measurements described below.

"Pairwise" far field patterns provide an even more direct means of estimating the relative phases of two adjacent lobes. An observation of a pairwise pattern is accomplished by blocking off all but the two lobes that are of interest to us with a pair of beam blockers, right after the laser beam has emerged from the output coupler mirror. A series of these pairwise far field patterns captured on the scope are displayed in Figure 2-5, starting with the pair from the left end of the array. It is interesting to note that the disparity between the two far field peaks is

the smallest in the middle region of the array and grows towards each end. Later in Section 3.4, we will estimate the phase profile of the field [in the array] from this figure and interpret it along with other data.

Incidentally, with input power at ~ 1000 W and pressure at 80 torr, the maximum power obtainable from this eight-element laser was approximately 45 to 50 W, which is a substantial dropoff from typical power outputs of about 70 W for an uncoupled array of similar size [assuming 0.4 % one-way intracavity loss]. The laser maintained its phase-locked operation, i.e., the output was of single frequency, through a substantial amount of PZT tuning.

As described earlier, cavity lengths can be varied, to a certain extent, by controlling the PZT voltages. Between the PZT located at the maximum reflector end, hereafter termed "length" PZT, and the PZT at the output coupler end, termed "tilt" PZT, moving the latter clearly yielded more interesting results. Although varying the length PZT voltage did result in a change in the output power, it did not significantly change the shape of the intensity distribution in the array. Varying the tilt PZT voltage, however, not only affected the overall output power level, but also shifted the peak of the array intensity toward one side, the side where the distance between the waveguide and the end mirror is reduced as a result of the tilt [see Figure 2-6 for example]. Output power was maximum when the peak was in the middle and decreased sharply when the mirror tilt deviated from that position. It is worth noting that the maximum displacement of the mirror [across the array] brought about by the tilt PZT is only on the order of a few μm; this will be an important clue for us when we try to explain the device's response to a tilt in Section 3.3.

In an effort to determine whether the end elements play a critical role in shaping the array intensity distribution, the following experiment was conducted. A thin piece of ceramic - made of Al_2O_3, as is the waveguide - just large enough to match the dimensions of the end elements was gently lodged in one of the end elements near the output coupler end. As the ceramic is highly lossy at 10.6 μm, this represents a very large loss for the wave in that element. The result was a dramatic reduction in the output power - down to about 15 W - , accompanied by a shifting of the intensity distribution away from the side with the lossy element, as shown in Figure 2-7a. Note that no power is coming from the leftmost element and a very small amount from its immediate neighbor. Compare this to Figure 2-3. Because of the way the geometric configuration of SHB arrays forces the field in one channel to be coupled with those from the other channels, the ceramic piece affected not only the field in the end element, but also the field in the rest of the array as well.

Also, note from Figure 2-7b that the far field scan shows a far greater degree of asymmetry between the two peaks compared to the case without the ceramic piece [cf. Figure 2-4], suggesting that the phase profile of the field in the array has deviated from that of a pure EH_{21} mode even further than before. This is further substantiated by a series of pairwise far field pattern photos shown in Figure 2-8. Note how large the disparity between the two peaks is in each photo [compare these to the previous results with no ceramic piece in Figure 2-5] and how it grows

Figure 2-3 Near Field Intensity Scan of the Eight-Element SHB Array

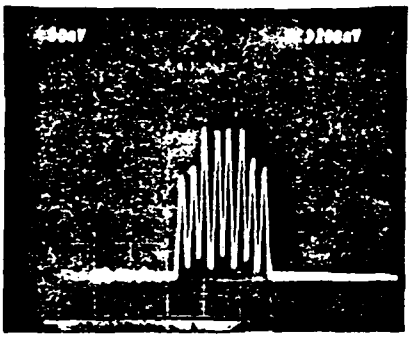

Figure 2-4 Far Field Intensity Scan of the Eight-Element SHB Array

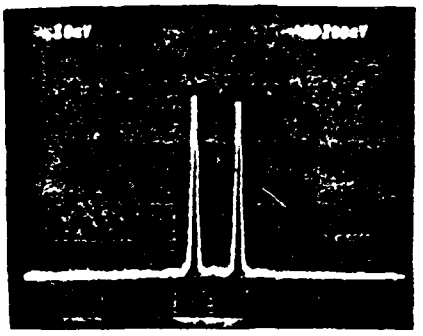

Figure 2-5 Pairwise Far Field Patterns of the Eight-Element Array

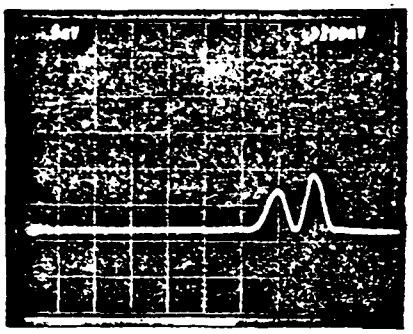

1+2

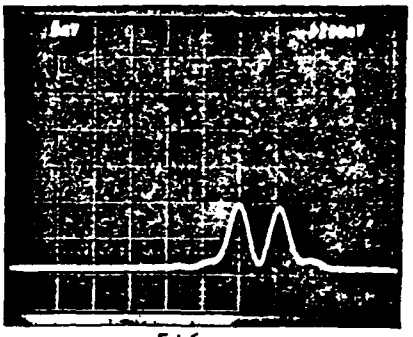

5+6

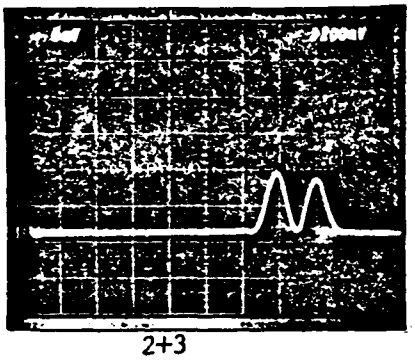

2+3

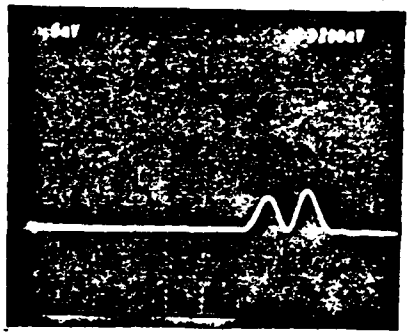

6+7

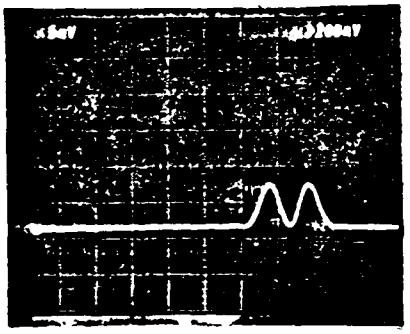

3+4

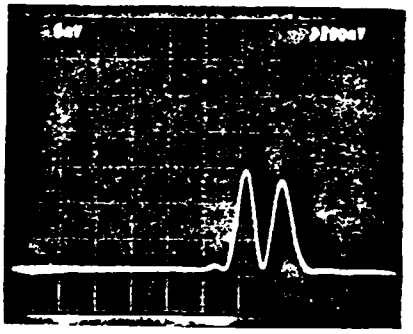

7+8

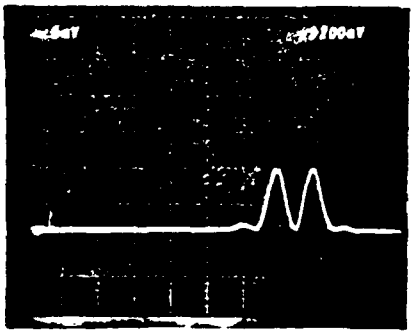

4+5

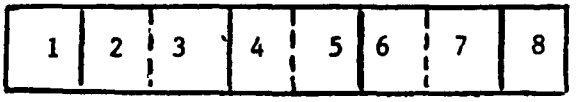

END VIEW OF THE ARRAY

Figure 2-6 Effect of a Tilt on the Near Field Pattern

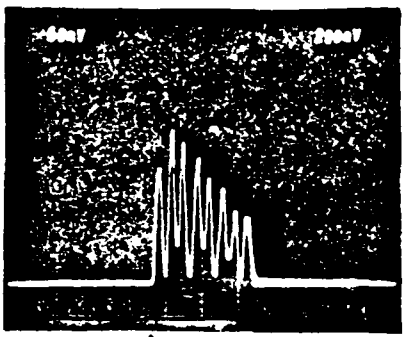

THE END WHERE THE MIRROR IS
IS MOVED CLOSER TO THE ARRAY

Figure 2-7 Near and Far Field Scans of the Array with a Ceramic Piece in Channel 1

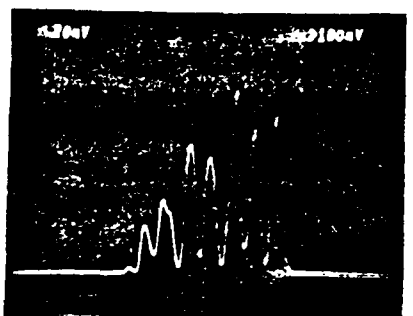

NO POWER OUT OF THE
LOSSY ELEMENT

(a) Near Field Scan

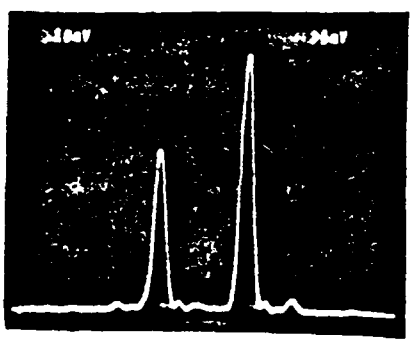

(b) Far Field Scan

Figure 2-8 Pairwise Far Field Patterns for the Lossy Eight-Element Array

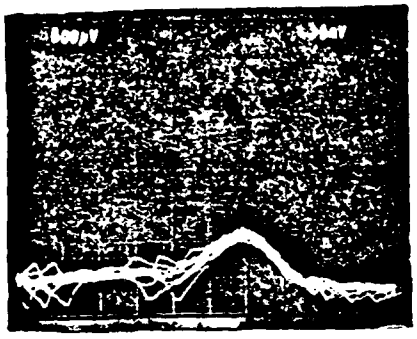

1+2

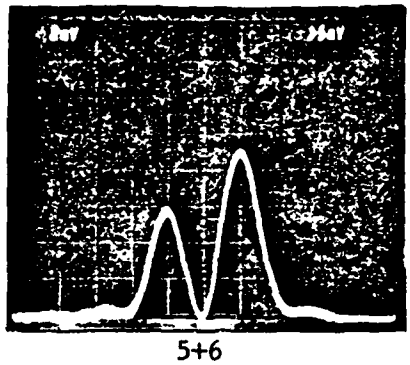

5+6

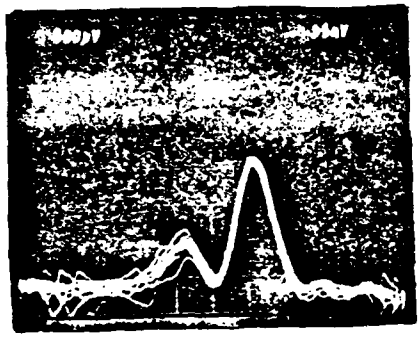

2+3

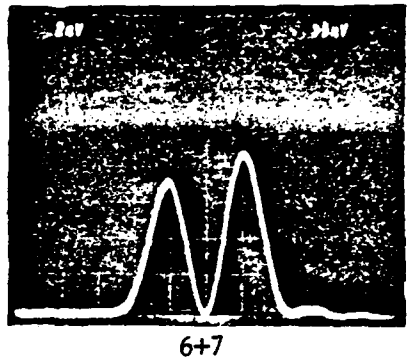

6+7

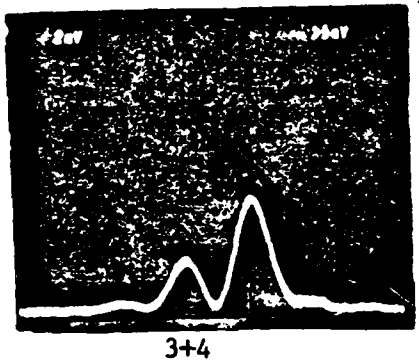

3+4

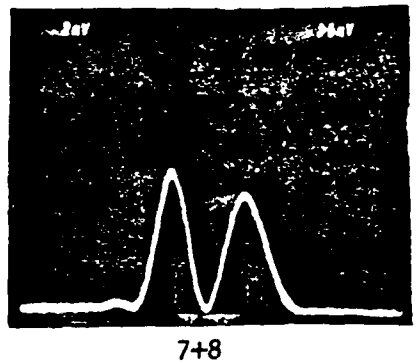

7+8

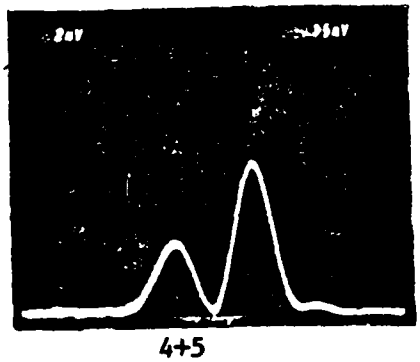

4+5

toward the end with the lossy element.

This experiment involving insertion of a ceramic piece into the laser was repeated with a larger ceramic piece, this time lodged in the center channel spanning elements 4 and 5. This time, the suppression of the output power was almost complete; the meter reading registered less than 1 W. It seems that because of the symmetry, a large intracavity loss in the middle portion of the array reduces the output power much more efficiently than a similar loss in the end channel. In any case, this finding could have some important implications, and they will be discussed in Section 4.

2.2 Experimental Results for a Two-Element Array

Many interesting features were observed with the eight-element array. However, because there are many elements in the array, it is difficult to isolate the effects of a single mechanism in such an environment. The two-element array shown in Figure 2-9 was constructed just for that purpose. The guide dimensions were 44 mils x 87 mils each and the dividing wall' thickness was about 10 mils.

One of the original goals set for the two-element array experiment was to study its phase-locking behavior as a function of the coupling length [l_c in the figure]; the coupling length would be increased in discrete steps by incrementally removing the dividing aperture wall.

With the entire dividing wall in tact - except for a little chip at one end measuring about 5 mm -, phase-locked behavior was witnessed for a small range of PZT adjustments. The pictures in Figure 2-10 correspond to the far field intensity pattern of the "in-phase" phase-locked mode, the "out-of-phase" phase-locked mode, and finally, the unlocked mode, respectively. The in- and out-of-phase modes are named so because the fields in the left and the right half of the array had to be in and out of phase with each other, respectively, in order to produce such far field patterns. It is somewhat surprising that the two elements can be locked together at this point, given that the coupling due to the chip and the the diffraction coupling due to the [small] gap between the waveguide and the end mirror are probably quite weak.

As mentioned earlier, it had been hoped that the output power and the locking-range could be measured as a function of the coupling length. However, the latter turned out to be a challenging problem; due to a very strong coupling between the two elements, it was nearly impossible to unlock the array without its breaking into higher order [spatial] modes for coupling length of 5 cm and beyond. Measurements of the locking range Δf_{lock} versus the input power and pressure were obtained at l_c = 2 cm and the results are presented in Table 2-1. The rf power dependence is not immediately obvious, but the data clearly indicate that the locking-range increases with the pressure.

Table 2-1 Locking Range Δf_{lock} vs. Input Power, Pressure

Pressure (torr) \ P_{in}(W)	250	275	300	325
70	0.6 MHz	0.7 MHz	0.7 MHz	
90	1.0 MHz	0.9 MHz	1.0 MHz	1.0 MHz
110	1.5 MHz	1.3 MHz	1.3 MHz	1.5 MHz

[Coupling Length = 2 cm]

Next, a parametric study was performed to measure the output power's dependence on the coupling length. Table 2-2 below shows the maximum power obtained for the array for various coupling lengths with the rf power P_{in} at 300 W and the pressure p at 100 torr.

Table 2-2 P_{out} vs. Coupling Length

P_{out}(W) \ Coupling Length (cm)	0	2	5*	10	20	30
	17-18	18	17	13-15	7-8	7-8

[P_{in} = 300W (325*), Pressure = 100 torr]

It appears that P_{out} decreases with the coupling length. However, these numbers should be accepted with some caution. The above measurement was plagued time and time again by the problem of partial discharge, viz., only a part of the array would have a full gas discharge. In fact, the power meter readings either fluctuated quite a bit in some instances - this was definitely not due to the usual thermal tuning process - or changed from one trial to the next. Therefore, we believe some of the measured output power values were probably lower than they ought to have been.

One major reason for studying a two-element array, besides its structural simplicity, was its symmetry. Because of the symmetry between the two halves, it seems reasonable to expect whatever physical conditions that exist on one side of the array, such as the temperature distribution, to prevail on the other side as well. This would mean that the tilt PZT could be used to produce any desired - within limits of the allowable PZT extension - difference in the effective cavity length between the two elements and that the array's response could then be monitored to find, if

any, correlations between them. This was done with the coupling length at 5 cm and pressure at 100 torr. Summary of the results are described below, but first a comment on the measurement procedure that was employed.

First, the output power was maximized with respect to tilt and length (PZT) adjustments. Presumably, the two elements of the array have equal effective cavity lengths at this point. Then, various amounts of tilt were applied from this quiescent point and the change in the output was recorded. [The actual amount of tilt inside the laser was estimated by using a setup that utilized a HeNe laser at a distant location and its reflection off a small mirror attached to the laser's mirror mount. A digital multimeter was also used to monitor the applied voltage to the PZT] Table 2-3 shows the effect of tilt on the output power, while Figure 2-11 depicts how the far field scans were affected. Corresponding near field scans are displayed in Figure 2-12. The swing in the cavity length difference over the full range of tilt PZT adjustment is approximately 1 μm. In the table, Δl is the [one-way] path length difference between the two elements that was induced by the tilt.

Table 2-3 P_{out} vs [Tilt-Induced] Cavity Length Change

	Δl (μm)				
	0.0	0.263	0.394	0.659	-0.362
P_{out}(W)	18	16	11	7	11

[P_{in} = 325-345 W, Pressure = 100 torr, l_c = 5 cm]

From examining the table and the figures, a few things are immediately obvious. One, a tilt to either direction, from the maximum-output-power-position, produces a rather sharp drop in power. Two, the drop in output power is accompanied by a similarly noticeable change in the far field pattern; in particular, the symmetry of the twin-peak pattern gets increasingly distorted with a greater amount of tilt. Three, the near field distribution seems to be affected by the tilt only to the extent that it is scaled down; the degree of symmetry does not appear to change much. And four, only the out-of-phase mode is observed. In fact, this is true for any coupling length [except l_c = 0]. This is plausible since the out-of-phase mode has a lower loss at the dividing wall, owing to its weaker intensity in the middle of the array.

2.4 Experimental Results for a Ten-Element SHB Array

The experiment with the eight-element array shed light on some, rather important behaviors of phase-locked SHB arrays, in particular the effect the cavity length variations have on the output power and the intensity and phase profile of the field. These findings were given

Figure 2-9 Structure of the Two-Element Array

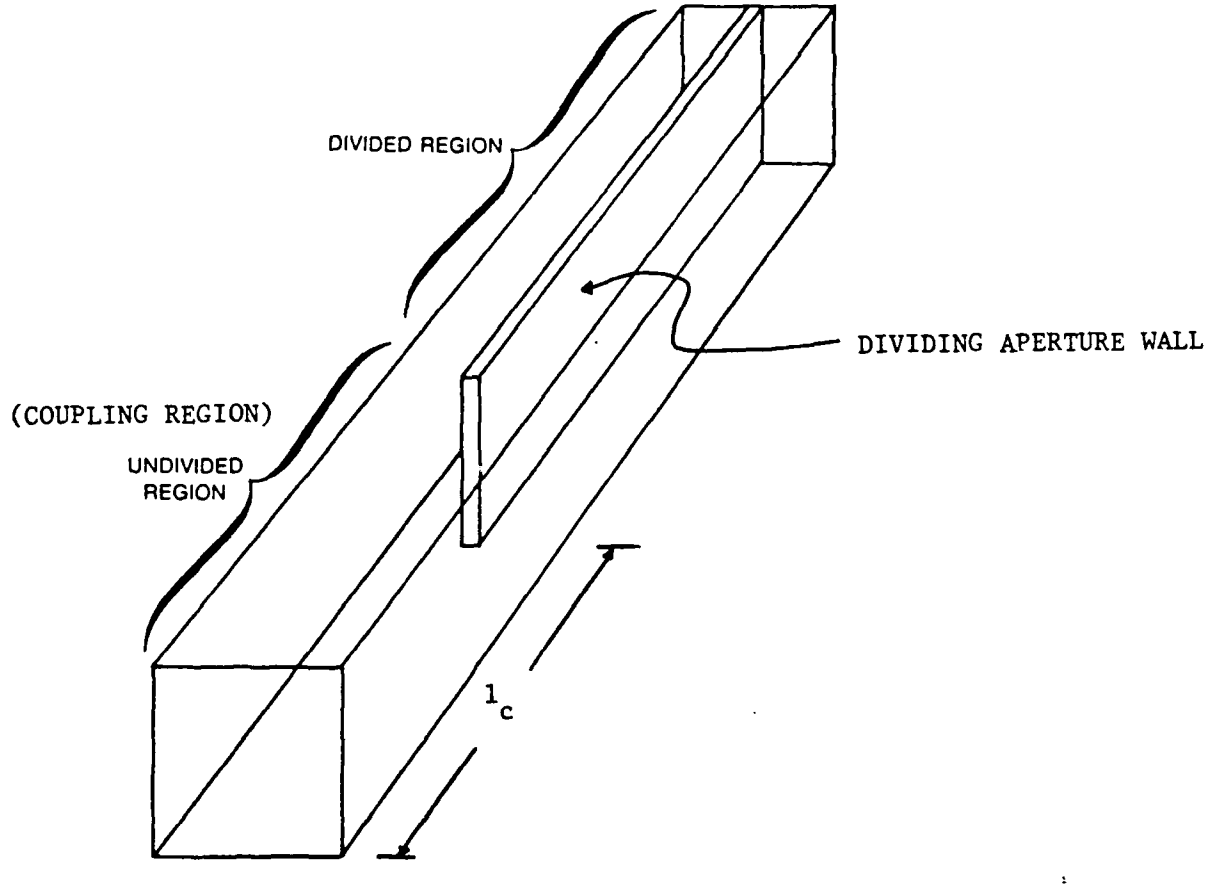

Figure 2-10 Far Field Patterns of the Two-Element Array ($l_c = 0$)

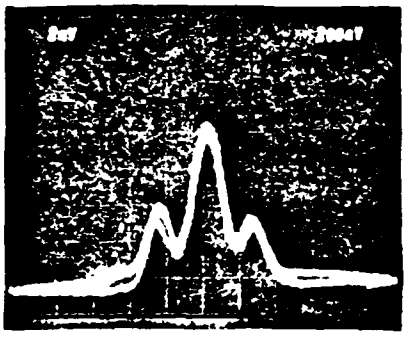

(a) In-Phase Mode (Locked)

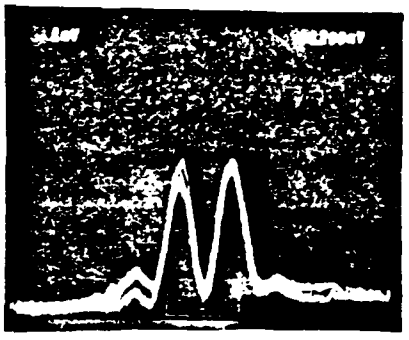

(b) Out-of-Phase Mode (Locked)

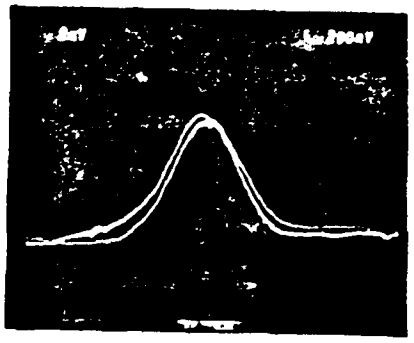

(c) Unlocked

Figure 2-11 Effect of a Tilt on the Far Field Pattern

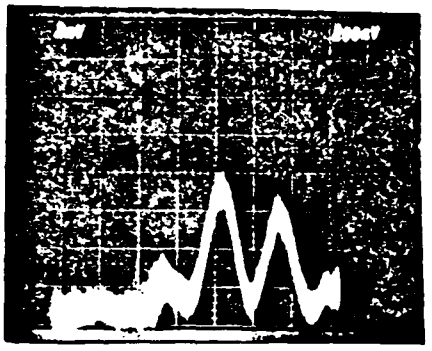

$\Delta l = -0.49\ \mu m$

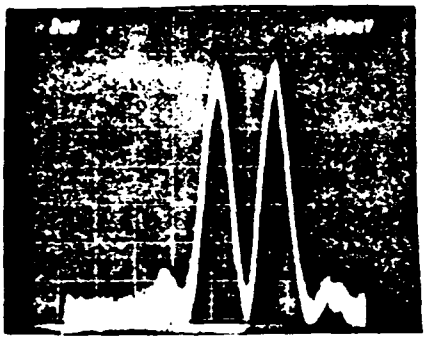

$\Delta l = 0\ \mu m$

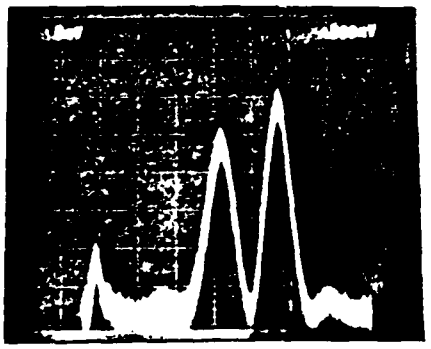

$\Delta l = 0.33\ \mu m$

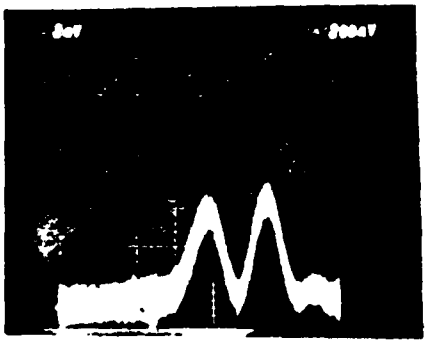

$\Delta l = 0.72 \mu m$

Figure 2-12 Effect of a Tilt on the Near Field Pattern

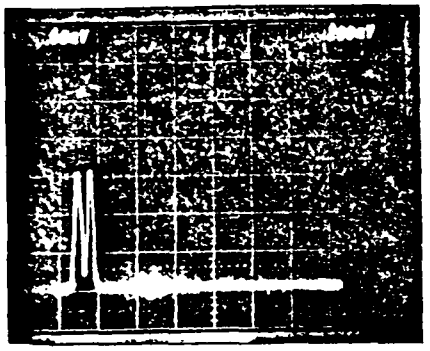

$\Delta 1 = -0.49\ \mu m$

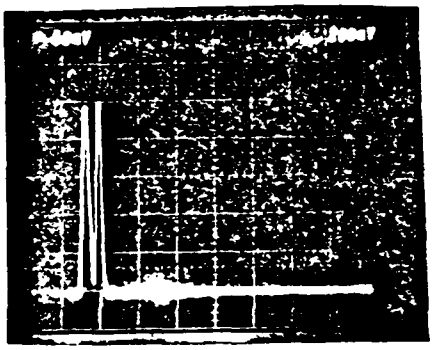

$\Delta 1 = 0\ \mu m$

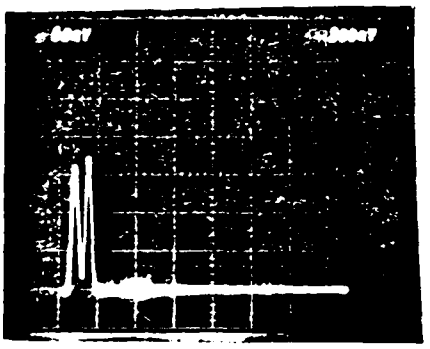

$\Delta 1 = 0.33\ \mu m$

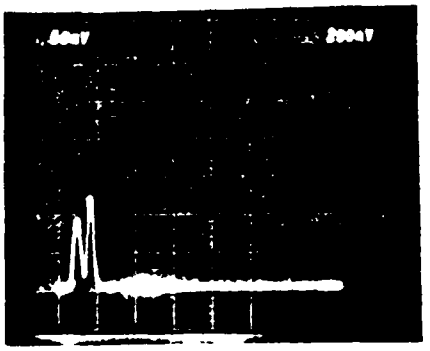

$\Delta 1 = 0.72\ \mu m$

further support by the results of the experiments performed on the two-element array, and will provide much of the basis for our effort in Section 3.3 in formulating a theory on the underlying mechanism responsible for SHB array's behavior in phase-locked regime. In the last portion of the experimental phase of our program, a ten-element SHB array was fabricated and tested, with the main goal of providing an opportunity to test the model based on the preceding two- and eight-element array results.

The ten-element array, as it was first delivered from the shop, was not in the SHB configuration, with all ten elements completely separated by the dividing walls along the waveguide. And before the waveguide was altered to conform to the SHB array structure, two sets of measurements were made.

The first set of measurements were made with the array untouched, in the original shape; these measurements would later be used as a reference with which to compare the results of the phase-locked SHB array. First, minimum spread of frequencies Δf_{min} (cf. [1],[3]) was measured as a function of pressure. With the nominal input power at 1 kW, Δf_{min} was estimated to be about 40, 40, 80, and 110 MHz for pressures of 70, 80, 90, and 100 torr, respectively. The rationale behind this measurement was that Δf_{min} would most likely correspond to the beat frequency between one of the end elements and one of the inner elements because cooling is probably most efficient near each end, and therefore we may get a crude estimate of the spread of the refractive index in the array and also the effective cavity length variations [ignoring the actual physical cavity length variations that may exist in the array for the moment]. Our hypothesis regarding the end elements being cooled more efficiently was justified somewhat by an additional set of measurements, which were obtained under the same set of circumstances as the last set; the only difference was that now the end element from each side of the array was not lasing. The corresponding Δf_{min} was 35, 25 and 40 MHz for p = 70, 80, 90 torr, respectively [measurement unavailable for 100 torr]. Clearly, the minimum spread of frequencies is a lot smaller without the end elements, suggesting that the inner elements have more a uniform index profile. This rather fortuitous [?] event was caused by a recurrence of the uneven discharge distribution problem; as will be mentioned shortly, the end elements had either a very weak discharge or none at all in certain cases.

Next, the near field and far field scans were taken at P_{in} = 1000 W for various pressures (see Figure 2-13); since the far field pattern did not change much with this uncoupled structure, only one was included. It is interesting to see how the uniformity of the near field distributions at lower pressures gives way to odd-looking profiles as the pressure is increased. In particular, the intensity at the end elements became progressively weaker with increasing pressure, and at 120 torr, we witnessed a very curious feature involving the intensity being stronger at every other element. Tilt PZT adjustments do not seem to affect the intensity distribution too much, which is not surprising since there is no - or very little - coupling among the elements; tuning the length PZT results in a small change in the level of the near field scan without affecting its shape.

Given that the elements are not coupled together and that their losses must be very similar, we are led to believe that the cause of these nonuniform intensity profiles must be a nonuniform discharge distribution in the array. Unfortunately, it is not clear at this time why the discharge [density] is not uniform in some cases. The uneven discharge problem is troublesome in that under such a condition, output power cannot be extracted to its fullest potential. From an analytical standpoint, the nonuniformity may make it difficult for us to distinguish the phase-locking-induced effects from the discharge-induced effects since the former could also cause a nonuniform intensity profile. However, the laser could perhaps be operated in a low pressure, high rf power regime, where the discharge distribution is likely to be more uniform, so that any discharge-related effect may be minimized.

The last parametric study conducted with the uncoupled ten-element array was that of the output power vs. rf power and pressure; Table 2-4 allows a quick look at the results. Whereas the correlation between the input power and the output power seems obvious - at least in this regime - the pressure dependence is not very clear.

Table 2-4 Output Power vs Input Power, Pressure: Uncoupled Ten-Element Array

Pressure (torr) \ P_{in} (W)	800	950	1100	1250
80	52	59	66	70*
90	48	60	68	74*
100	46	54	64	74

[* P_{in} = 1200 W]

The second set of measurements were made after having removed about 5 cm from each dividing wall in an alternating fashion as shown in Figure 2-14; the walls separating the two end elements from the rest of the array were left untouched. The purpose of this particular move was to see whether an increase in output power and a more uniform array profile could be obtained - compared to the usual SHB array structure - by adopting this more uniform array structure. We say more uniform because, topologically, the channels in this arrangement are more alike [ignoring the end elements which were left uncoupled to the rest for comparison purpose] than in the ordinary SHB structure, where the end elements are quite different from the rest of the array.

Unfortunately, it was not possible to phase-lock [the inner elements] in this configuration despite considerable amount of effort. Furthermore,

Figure 2-13 Near and Far Field Patterns of an Uncoupled Ten-Element Array for Different Pressures

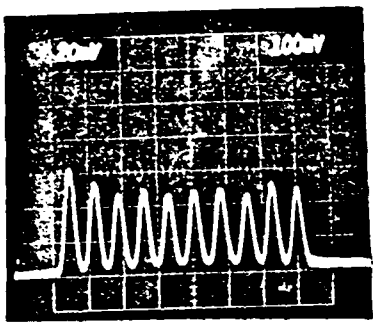

60 torr

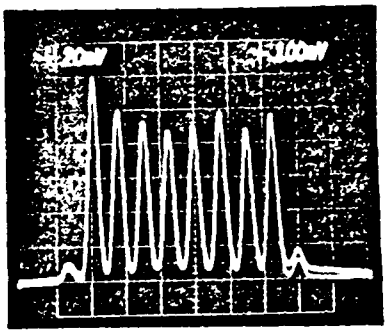

110 torr

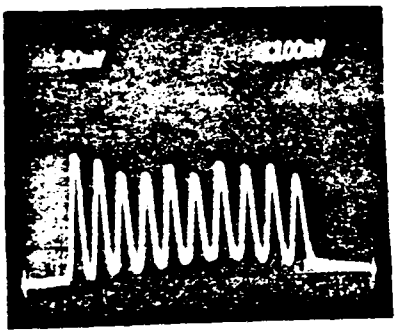

80 torr

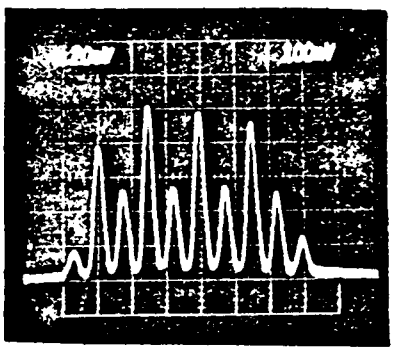

120 torr

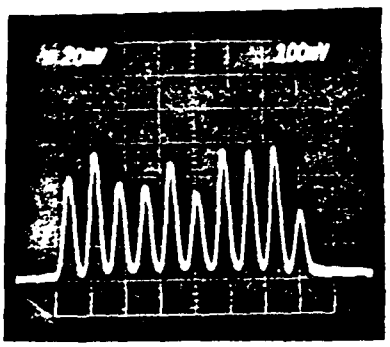

90 torr

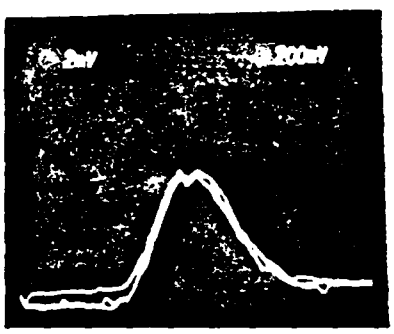

FAR FIELD PATTERN (80 torr)

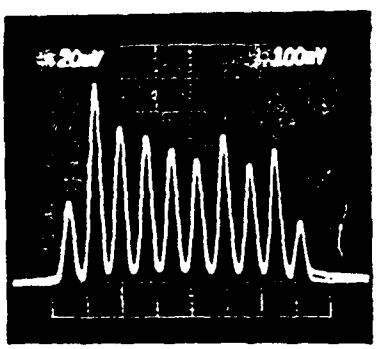

100 torr

Figure 2-14 Ten-Element Array with 5 cm Coupling

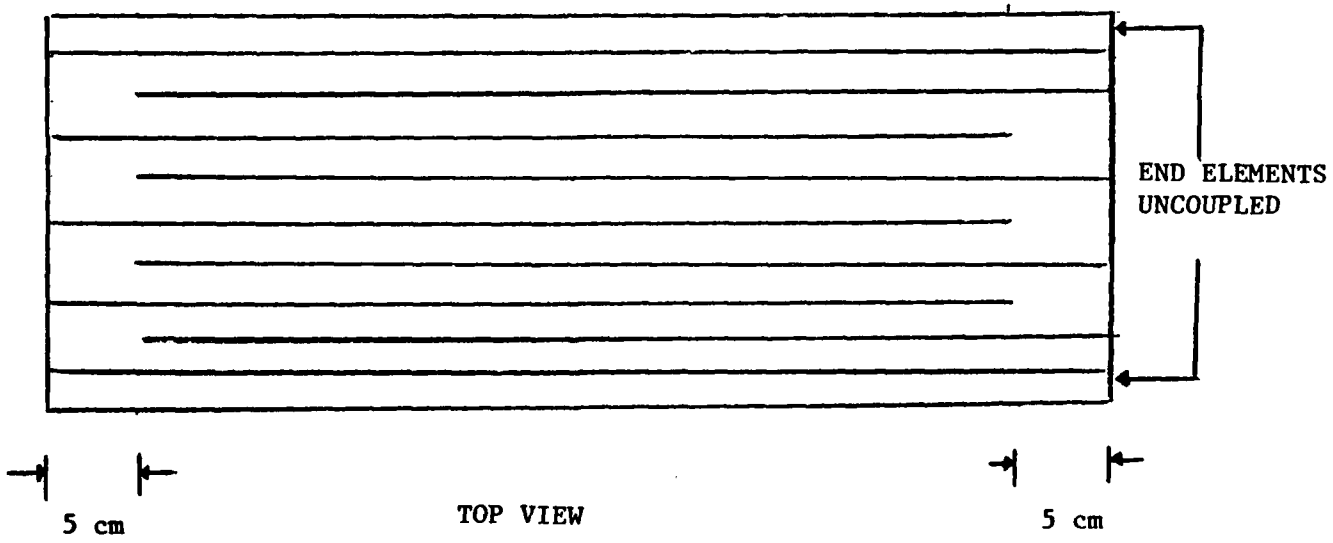

the near field scan and thermal plate images revealed that the field distribution in the array was not only highly nonuniform but also contained a lot of higher order mode content. At 90 torr, 1000 W of rf power resulted in only 20-25 W of optical power, which is less than half of the corresponding value for the previous uncoupled case. This dramatic decrease in output power in comparison to the no-coupling case may be chiefly due to the loss at the dividing aperture walls [to be termed mode mismatch loss later] and the discharge problem that we have encountered before.

After the preceding measurements were made, the array was finally transformed into the regular SHB array structure, with the coupling region occupying half of the waveguide length. First, a parametric study of P_{out} vs. P_{in} and pressure was conducted; its results are tabulated in Table 2-5 [The P_{out} values reported here were maximized with respect to tilt PZT adjustments]. Note the significant reduction in P_{out} across the board comapred to the no-coupling case [cf. Table 2-4].

Table 2-5 Output Power vs Input Power, Pressure: Ten-Element SHB Array

Pressure (torr) \ P_{in} (W)	800	950	1100	1200
80	34	40	38	34*
90	26	27*	41	38
100	23*	22*	30*	41

The entries with an asterisk(*) mark should be viewed with some skepticism as the problem of partial discharge is suspected in some of the guides for those cases.

Next, at the operating point of P_{in} = 1200 W and p = 90 torr, the effects of tilt PZT adjustments on P_{out}, near field and pairwise far field patterns were examined. The values for P_{in} and p were chosen so as to [hopefully] minimize the influence of uneven gas discharge distribution (see Figure 2-13) while maintaining a reasonable level of output power. Originally, measurements at several tilt positions were planned. However, difficulty in maintaining a clean mode pattern in single frequency made it necessary to take measurements at only two tilt positions, with the first position representing the maximum output power position and the second position representing the edge of phase-locked regime. When a tilt larger than the latter was applied, a single beat frequency appeared, with additional beats appearing upon further increase in the tilt. The angular separation between the first and the second tilt positions was estimated to be only about 80 μrad, equivalent to roughly 0.1 μm in terms of the change in the cavity length difference between a pair of adjacent guides. As a result, it was no great surprise that the two sets of data - one for

each position - were quite similar.

The output power for the two cases was measured at 38 and 34 W, respectively [44 W was observed at one time, but it could not be sustained]. This represents a substantial loss of power compared to the uncoupled case's 70 W, and may be, in part, related to the frequent signs of discharge problems and the alignment difficulties experienced during the measurement process.

Figures 2-15 and 2-16 are the photographed near and far field patterns at the first and second tilt positions, respectively; Figures 2-17 and 2-18 show the pairwise far field patterns for the two tilt positions, going from right to left in the near field pattern pictures. A few comments are in order regarding these pictures.

The effects of tilt on the array's near field intensity distribution are quite apparent seeing that the near field pattern for the second case - with a larger applied tilt - has a decidedly more lopsided appearance. The skewed near field pattern of the first tilt case suggests that the there may have been some amount of mirror tilt in the first place, perhaps introduced in the mirror alignment process prior to PZT tuning.

The two main lobes of the far field photograph are of different amplitudes in each case, indicating that the phase distribution of the field across the array does not really obey that of a pure EH_{21} mode, i.e., the phase of the field does not change by exactly 180° from one element to the next. Another visible evidence of the presence of other waveguide modes in each guide comes from the little peaks that lie outside the two principal lobes. These minature peaks, representing probably the EH_{41} mode component in the phase-locked mode, is more pronounced in the second case, which seems consistent with the findings of [6] correlating the extent of mirror tilt with fractional content of higher order waveguide modes in the resonator mode of a single waveguide. [By comparison, Figure 2-4 shows a very symmetric far field pattern with virtually no side peaks. Judging from the accompanying near field scan in Figure 2-5, amount of mirror tilt appears to have been minimal in that instance]

The two sets of pairwise far field pattern pictures in Figures 2-17 and 2-18 are similar in general: in each case, the first picture seems to have the most asymmetric pattern, indicating a large phase mismatch between the two weakest-intensity elements of the array. The last pairwise pattern of Figure 2-17 appears to be anomaly.

Figure 2-15 Near and Far Field Patterns of a Ten-Element SHB Array (I)

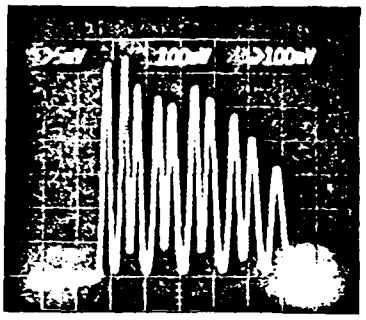

Near Field Pattern

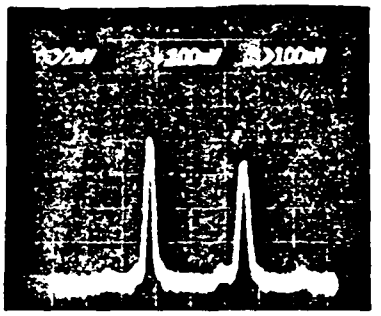

Far Field Pattern

Figure 2-16 Near and Far Field Patterns of a Ten-Element SHB Array (II)

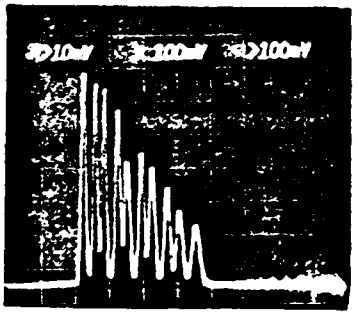

Near Field Pattern

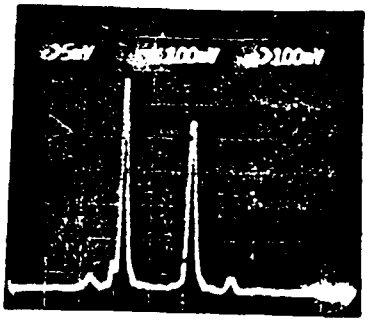

Far Field Pattern

Figure 2-17 Pairwise Far Field Patterns of a Ten-Element SHB Array (I)
(Starting from the rightmost pair of lobes in Figure 2-15)

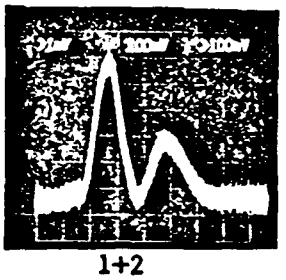

1+2

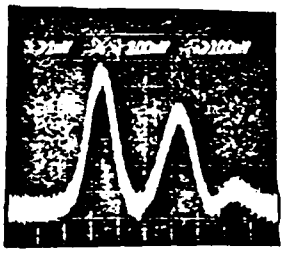

2+3

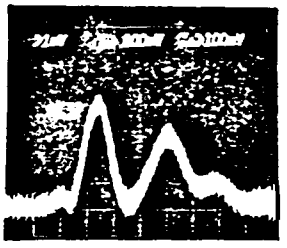

3+4

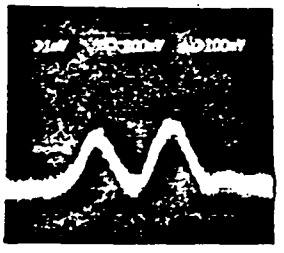

4+5

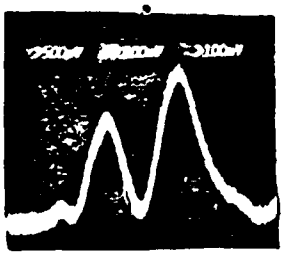

5+6

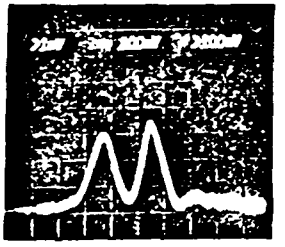

6+7

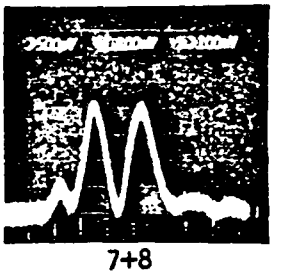

7+8

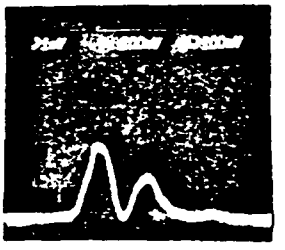

8+9

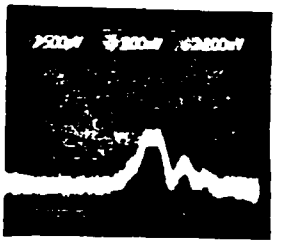

9+10

Figure 2-18 Pairwise Far Field Patterns of a Ten-Element SHB Array (II)
(Starting from the rightmost pair of lobes in Figure 2-16)

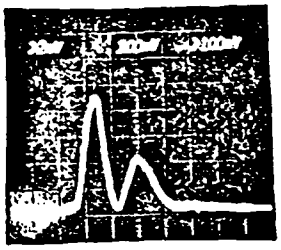

1+2

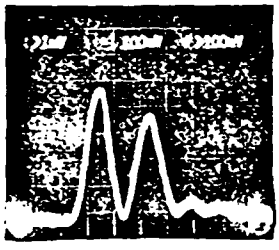

2+3

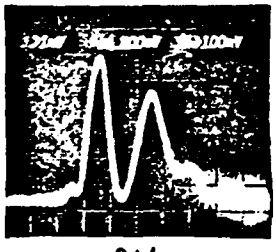

3+4

4+5

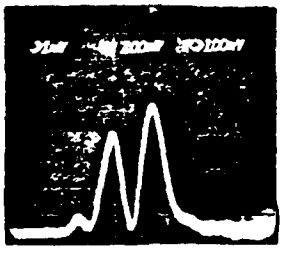

5+6

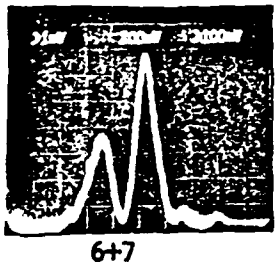

6+7

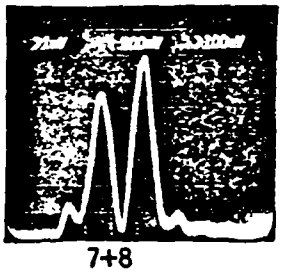

7+8

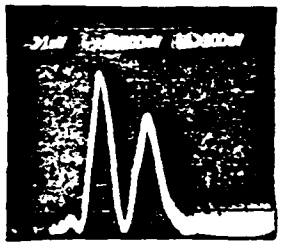

8+9

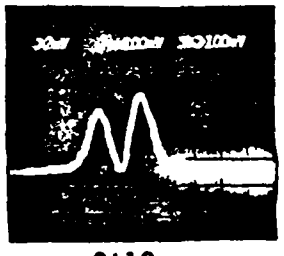

9+10

3.0 DESCRIPTION OF THE THEORETICAL EFFORT

3.1 Introduction

The main focus of the theoretical effort in the program was placed on gaining a better understanding of the observed experimental results so that improvements can be made on the present performance level. In particular, a theoretical model of SHB array lasers should be able to address the nonuniform profile of the array intensity and the role of cavity length variations in determining the array's general behavior.

Section 3.2 describes the primary loss mechanisms of SHB array lasers - most importantly the mode mismatch loss - and presents the calculations of their approximate numerical values, along with a few comments on their sensitivity to perturbations in general. It is followed by Section 3.3, whose first segment describes a rigorous approach to finding, at least in principle, the exact supermodes and the associated roundtrip gains of a passive SHB array. The remainder of the section features a recent theory on locking behavior of phase-locked arrays, which is based on apriori knowledge of the array's supermodes. Section 3.4 keys on establishing a relationship between effective cavity length variations and the array laser's behavior, based on the findings of Sections 3.2 and 3.3 and the experimental results of Section 2. In particular, possible connections to the output power, the phase profile of the array, and the near field intensity profile are investigated.

The following is a summary of the progresses made in the theoretical portion of the program.

1) Identification and estimation of the primary losses in a SHB array laser.

2) A detailed examination of the mode mismatch loss: its origin and its dependence on the amplitude and phase mismatch between the fields in adjacent guides.

3) Formulation of a theory on the behavior of a phase-locked SHB array based on the mode mismatch loss mechanism.

4) Explanation of several key features of the experimental data using the theory developed herein.

5) Estimation of the phase profile of the field in the array from the pairwise far field patterns.

6) Formulation of a theoretical approach to finding the supermodes of a [passive] SHB array.

7) Application of a phase-locking theory on planar coupled cavity lasers to SHB arrays.

In summing up the theoretical effort, some success has been achieved in explaining many of the features observed in the experimental portion of the program; however, our model is still short of being a unified and comprehensive model that can confidently predict the performance of SHB array lasers.

3.2 Primary Loss Mechanisms

Because the amount of output power delivered by a laser is directly affected by the losses incurred by the laser beam, importance of a good understanding of the loss mechanisms cannot be emphasized enough. In this section, primary sources of loss for SHB arrays will be reviewed and their numerical values estimated.

There are four main loss mechanisms for SHB arrays: (1) propagation - or "wall" - loss; (2) end mirror coupling loss; (3) output coupling loss; and (4) mode mismatch loss. The propagation loss is simply the loss incurred by the wave due to its interaction with the guiding walls as it propagates down the guide. It is a well-understood problem, which has been analyzed extensively in the past [7], including in the previous reports by UTRC on "Coupled High Power Waveguide Laser Research Program" [3]. The end mirror coupling loss refers to the power that is not coupled back into the array after reflecting off the end mirrors. Its study has been confined mainly to the context of a single waveguide [6,8,9]. Output coupling loss is just the loss of power to the external environment through the coupler mirror. The mode mismatch loss refers to the loss which occurs when a propagating field from one section of the array does not exactly "fit" into the guide in the next section and as a result, some of the field is absorbed by the front of the dividing aperture wall at the array's midplane [3]. Very rough, first order calculations of this quantity are given in [3]; here, we shall give a much more accurate and detailed account of the loss. We may add that the mode mismatch loss arises because of the staggered structure of SHB arrays. [It is also conceivable that a reduction in gain may occur in transition from a phase-unlocked state to a phase-locked state, perhaps because the phase-locked frequency has been pulled away from the peak region of the gain curve. However, as this gain reduction would not be a real loss, it will be not included in the analysis here.]

Robustness and reproducibility are important factors to consider when designing and fabricating a high-precision device such as a SHB array: we would like to know how sensitive the device performance is going to be with respect to perturbations in general. The propagation loss and the output coupling loss should not be too sensitive to small structural changes or temperature variations as these losses are determined primarily by the guide dimensions and the material properties of the guide and the mirror(s). The end mirror coupling loss can change significantly with the guide-to-end-mirror distance [6,8,9]; however, it is unlikely that the gap distance would change enough during the operation of the laser to make a difference. The mode mismatch loss depends critically on the thickness of the dividing aperture walls. It also depends indirectly on the effective cavity length variations, but that is a complicated issue and will be

addressed later in this section and again in Section 3.4.

Let us now try to estimate the actual numbers associated with each type of loss in our experiments.

The propagation loss calculations are straightforward. Assuming guide dimensions of 92 mils x 92 mils [47 mils x 92 mils for the two end elements] and the refractive index of the ceramic as $n = 0.64 + i0.037$ [3], numerical value of 0.23 % roundtrip loss [0.43 % for the end elements] is obtained for x-polarized EH_{21} mode of the 37-cm laser. [The y-polarized mode has a much higher propagation loss and almost never lases] It must be pointed out, however, that the figures given above represent only a lower limit of the actual values since an array supermode also contains higher order waveguide mode components as well, which have higher propagation losses. In fact, later calculations carried out in conenction with the mode mismatch loss analysis puts the typical roundtrip propagation loss estimate at about 0.7-0.8 % for the inner elements of the above case [wall thickness of 10 mils assumed], the difference from the earlier estimate of 0.23 % being the inclusion of non-EH_{21} waveguide modes.

For the end mirror coupling loss, we need to calculate the fractional amount of power lost due diffraction of the beam at both ends of the array, i.e., the portion of the reflected beam spilling outside the array's cross section. Given that the separation distance between the end mirror(s) and the end of the waveguide is only about 5 mm, the beam diffraction is expected to be minimal, certainly not enough to cause the beam from one channel to spread out beyond its immediate neighbors. This means that for the inner elements, only the portion of the beam that spills over the top and the bottom of the waveguide should contribute to the coupling loss; diffraction in the horizontal direction just causes the energy to be coupled into other guides of the array and is not a loss as far as the entire array is concerned. With the end elements, on the other hand, we need to include diffraction loss over three sides of the channel.

For simplicity, let us assume that the resonator mode consists solely of the EH_{21} waveguide mode and that the effect of tilt is negligible in this particular calculation. The Fresnel number N ($\equiv a^2/4\lambda d$, where a is the dimension of a square channel, and d the waveguide-to-mirror distance) for our inner elements is approximately equal to 27. Using the asymptotic result for the end mirror coupling loss developed by Boulnois and Agrawal [8]

$$\Gamma_{mn} \approx (m^2 + n^2)/6N^{3/2} \quad \text{for } N \gg 1 \qquad [EH_{mn} \text{ mode}], \tag{3.1}$$

it is possible to estimate the diffraction loss for our problem. For the inner elements, $\Gamma_{21} \approx 0.00116$ or 0.116 %, taking into account only the loss in the vertical direction. For the rectangular end elements, the Fresnel number N is about 7 and 27 in the horizontal and vertical directions, respectively. It then follows that the diffraction loss in this case is 0.116 % - in the vertical direction - plus 0.460 % - in the horizontal direction - for a total of 0.576 %. [For roundtrip loss calculations, these numbers would be doubled] Therefore, the end mirror coupling loss is quite small.

The nominal end mirror reflectivities are 99.6 % and 92 % for the maximum reflectivity mirror and the coupler mirror, respectively. Thus, the total output coupling loss can be taken as 8.4 %.

Exact calculation of the mode mismatch loss is difficult because the supermode of a phase-locked array consists of more than just EH_{21} mode and its composition is not known apriori. However, we can at least formulate a model which illustrates the dependence of the mismatch loss at the dividing aperture wall on the phase and amplitude mismatch between the two field components which are coupled into the joining guide. The result will be used in Section 3.4 to explain why a phase-locked SHB array inherently yields less output power than an uncoupled array of the same number of elements, and also to illustrate how effective cavity length variations may affect several other features of the array output. We now proceed to develop the model.

Suppose the incident field in one of the guides just past the midpoint of the array $z = L/2_+$ is approximated by (see Figure 3-1):

$$E_i(x) = \begin{cases} \sin(2\pi x/a) & \text{for } 0 \le x < a(1-\delta)/2 \\ 0 & \text{for } a(1-\delta)/2 \le x < a(1+\delta)/2 \\ R\exp[j\Phi]\sin(2\pi x/a) & \text{for } a(1+\delta)/2 \le x < a, \end{cases} \tag{3.2}$$

where

R = normalized field amplitude in the region $a(1+\delta)/2 \le x < a$,

Φ = phase deviation (mismatch) of the field from a pure EH_{21} mode.

The field in the region $0 \le x < a(1-\delta)/2$ and the field in the region $a(1+\delta)/2 \le x < a$ have entered the guide from two adjacent guides that are butted up against it at $z = L/2$; and they are clipped at the edges because of the dividing wall on each side of the guide. The null region - zero-field region - between $x = a(1-\delta)/2$ and $x = a(1+\delta)/2$ reflects the presence of the dividing wall which separates guides 2 and 3 [see Figure 3-1]. For brevity, the y-dependence of the field has been omitted.

$E_i(x)$ can be expanded in terms of the waveguide modes EH_{m1} of guide 1:

$$E_i(x) = \Sigma\, c_m E_m(x), \qquad m = 1,2,3,\ldots$$

where

$$E_m(x) = \sin(m\pi x/a), \tag{3.3}$$

c_m = expansion coefficient for the m-th mode

$$= \begin{cases} (1+R\exp[j\Phi])\cdot((1-\delta)\cos(\delta\pi) + \sin(\delta\pi)/\pi)/2, & \text{for } m = 2 \\ (\sin(m\pi(1-\delta)/2) - R\exp[j\Phi]\sin(m\pi(1+\delta)/2)) & \\ \cdot 4/\pi(4-m^2) - (1 + (-1)^m R\exp[j\Phi])\sin(\delta\pi) & \text{for } m \ne 2 \\ \cdot 2m/\pi(4-m^2). & \end{cases}$$

Upon propagating down the guide, reflecting off the end mirror - assume a perfect end mirror coupling for now - and propagating back to $z = L/2_+$, $E_i(x)$ is transformed into:

Figure 3-1 Approximate Field Distribution in a SHB Array: Effect of the Dividing Aperture Walls

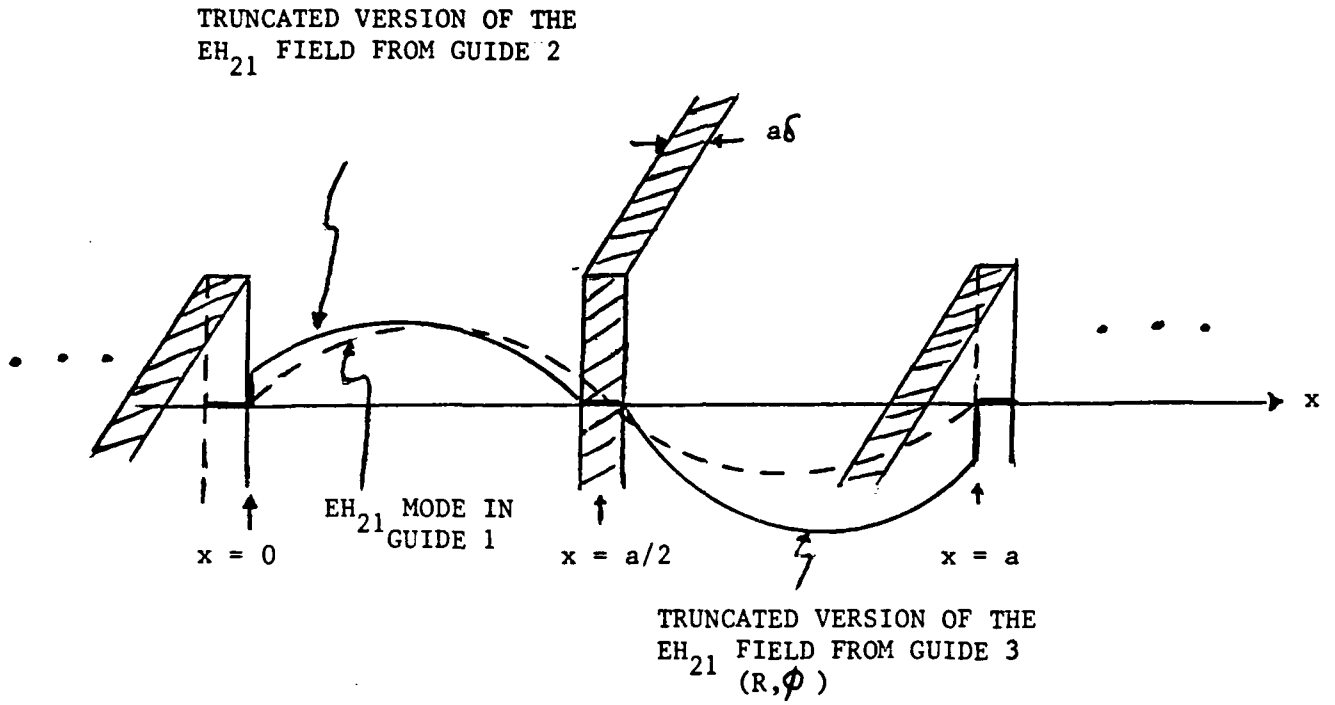

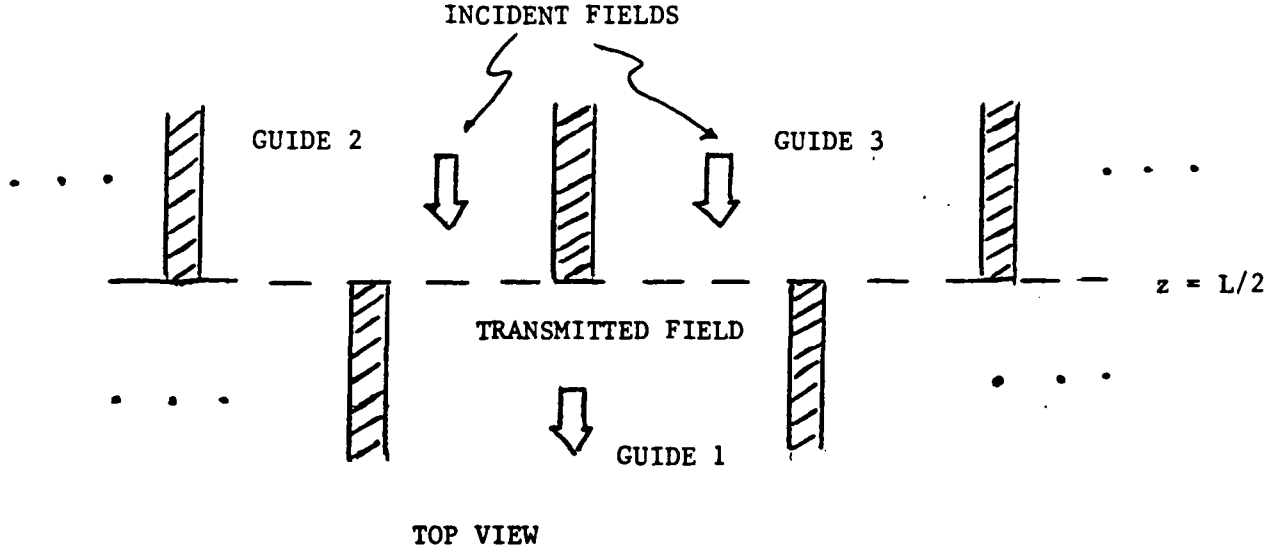

TOP VIEW

$$E_r(x) = \Sigma\, c_m E_m(x)\exp[jk_{m1}L], \tag{3.4}$$

where k_{m1} is the complex propagation constant of the EH_{m1} mode [7]. $E_r(x)$ will have a different field distribution from $E_i(x)$ since $E_i(x)$ is not a pure waveguide mode and the waveguide modes that make up $E_i(x)$ each have a different propagation constant. The portion of the return field $E_r(x)$ at the center of the guide will encounter a dividing wall and be absorbed; this is the mode mismatch loss that we alluded to earlier.

Strictly speaking, if the end mirror is tilted at some angle, nonuniform pathlength to the mirror across the guide will result in a rearrangement of the reflected field's mode composition [6]. However, here we shall assume that the tilt is negligible.

The fractional power loss due to absorption by the dividing aperture wall - extending from $x_- = a(1-\delta)/2$ to $x_+ = a(1+\delta)/2$ - is then given by

$$\Gamma_{mismatch} = \int_{x_-}^{x_+} dx\, |\Sigma\, c_m \exp[jk_{m1}L]E_m(x)|^2 / P_i$$

where (3.5)

P_i = incident power
$= a(1+R^2)\cdot((1-\delta)/4 + \sin(2\delta\pi)/8\pi)$.

Figure 3-2 displays the result of including up to 100 lowest modes in the expansion and computing the mode mismatch loss as a function of Φ and R. Note how large the mismatch loss can be even for a modest amount of phase mismatch. It shows that in general, increasing Φ introduces more and more of modes other than the EH_{21} mode and consequently leads to a larger loss at the dividing wall. The mismatch loss also increases with amplitude imbalance, i.e., with R [up to $\Phi = 90°$]. However, as the amplitude disparity becomes greater, the sensitivity of the fractional mismatch loss with respect to changes in Φ decreases; in fact, in the limiting case of $R \dashrightarrow \infty$, the fractional loss approaches a constant value. This makes physical sense because the $R \dashrightarrow \infty$ case represents a situation in which no power is coming from one of the guides and in that case the phase of the field in the other guide becomes irrelevant in the mode mismatch loss picture. Interestingly enough, the asymptotic value for this limiting case is also the value to which the mode mismatch loss converges for all R values at $\Phi = 90°$. The reason is that at $\Phi = 90°$, the fields originating from the left and right guides [guides 2 and 3, respectively] represent the in- and quadrature-phase components, respectively, and therefore couple independently into the waveguide modes of guide 1. The total mismatch loss in this case is then the sum of the mismatch losses for each component. Since the fractional mode mismatch loss for each half is independent of its field amplitude [according to the $R\dashrightarrow\infty$ result], their sum also retains this property.

Incidentally, clipping of the incident field by dividing aperture walls affects the propagation loss as well. This is because the clipping process, independent of the amplitude and phase mismatches - introduces higher order modes into the field; generally, thicker the wall, more power goes into the higher order modes. As a result, the total propagation loss - obtained by summing over different waveguide modes' contributions - was

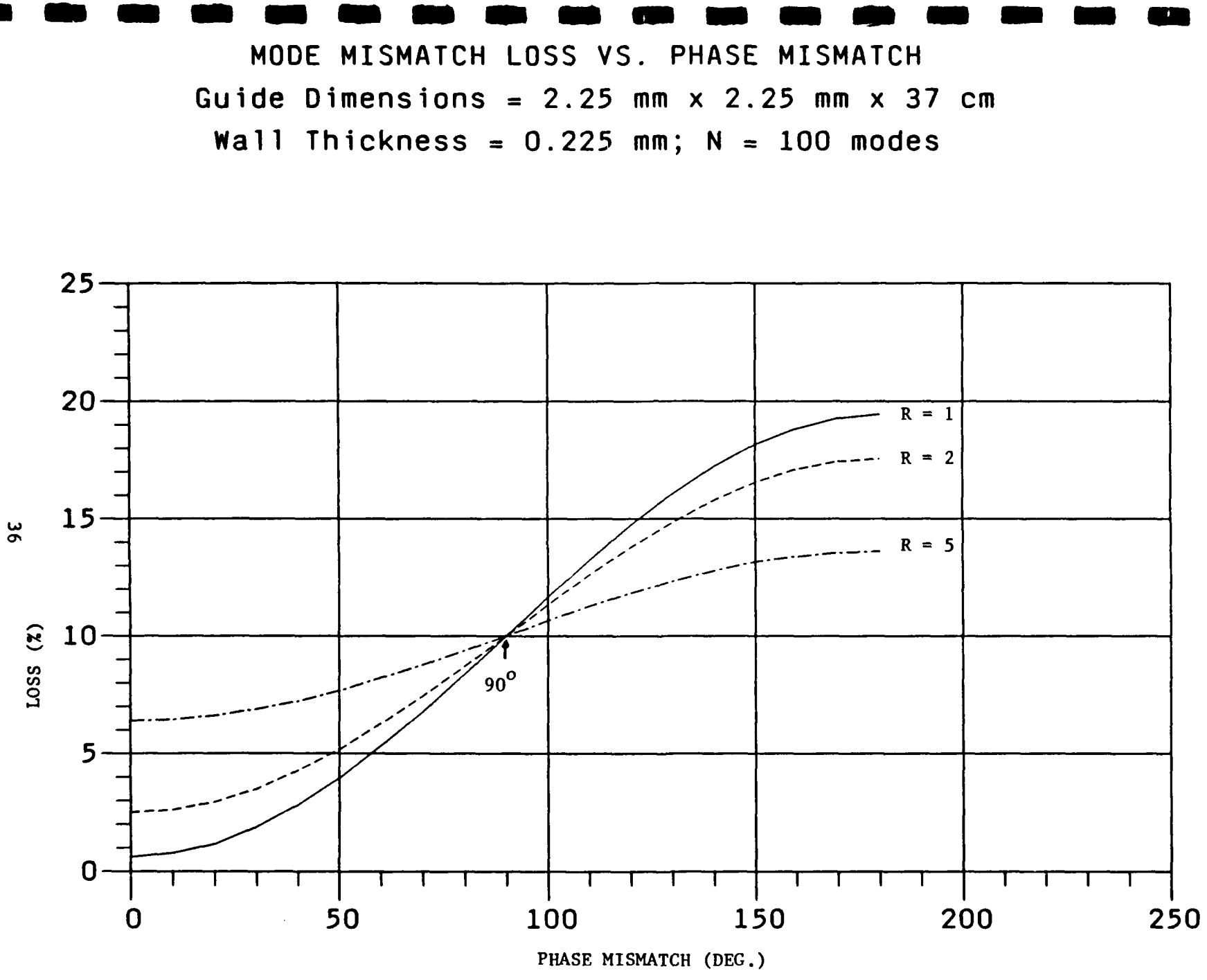

Figure 3-2 Effect of Amplitude and Phase Mismatch on the Mismatch Loss

considerably greater than the propagation loss of a pure EH_{21} mode. However, when compared to the [corresponding] mode mismatch loss, the propagation loss usually turned out to be insignificant. Oddly enough, though, the propagation loss appeared to be virtually independent of Φ and R values so long as the value of the propagation loss itself was small. We started to analyze this phenomenon in closed form but have not been able to complete the analysis in time to include in this report.

As a side remark, it is important to distinguish the [incident] power coupled into the non-EH_{21} modes from the actual power lost due to absorption at the dividing wall, i.e., the mode mismatch loss. The former can contribute indirectly to the latter by increasing the amount of beam diffracted onto the central portion of the guide, but it is not a physical loss in itself. In general, the latter is substantially smaller than the former.

Based on the preceding analysis, a lower bound estimate on the mismatch loss of a SHB array may be made by assuming a perfect match in the field amplitude and phase between all the elements, i.e., by assuming $\Phi = 0$ and $R = 1$. In all likelihood, however, the actual mismatch loss is expected to be much higher than such estimate for two main reasons: (1) The magnitude of Φ can be quite large, as seen in some of the pairwise far field patterns earlier; and (2) The non-EH_{21} waveguide modes probably make up a larger fraction of the phase-locked array mode than we have assumed above, which means greater mismatch loss. Recall that our analysis here had assumed a perfect EH_{21} mode in each of the two guides from which the collective incident field $E_i(x)$ emerges; of course, that is only an ideal approximation. More accurate estimate of the array's mode mismatch loss requires information regarding actual Φ and R values, which may be obtained from the near field pattern and the pairwise far field patterns.

Finally, a few comments on the sensitivity of the mode mismatch loss to changes in guide dimensions. The mismatch loss is quite insensitive to guide length changes of up to seveal cm's in typical structures. The reason for this is that the separation between the propagation constants of different waveguide modes is not very large, and thus a small change in the guide length has a minute effect on the overall field distribution. On the other hand, a small change in the guide width can have a dramatic impact. This is due to the fact that the propagation constant of a waveguide mode has a strong dependence on a and b, the guide width and height: $\beta_{mn} = k - ((m\pi/a)^2+(n\pi/b)^2)/2k$ for the EH_{mn} mode [k = wavenumber]. The strong $1/a^2$ dependence, coupled with the fact that each propagation constant is affected differently by a perturbation [to a and b], can radically change the appearance of the return field $E_r(x)$ and the mode mismatch loss from before. For example, consider that the minimum mismatch loss at $\Phi = 50°$, i.e., with $R = 1$, is calculated to be 2.86, 1.23, 2.84, 4.19, and 7.75 % for guide width of 1.8, 2.0, 2.2, 2.4, and 2.6 mm, respectively [37 cm guide length, 2.3 mm guide height, and wall thickness equal to 10 % of the guide width assumed]. These rapid changes demonstrate how critical the guide mensions are in determining the mode mismatch loss. As far as the wall thickness is concerned, we find that, not surprisingly, a thicker dividing wall leads to an increase in the mismatch loss in a monotonic fashion.

To summarize this section, the major sources of loss in a phase-locked SHB array laser have been identified as mode mismatch losses. The results of this section will be applied toward explaining some key features of phase-locked SHB array's behavior in Section 3.4.

3.3 Phase-Locked Arrays

There are two ways one can look at phase-locking of an array. One such view treats the modes of a phase-locked array as a slightly perturbed version of the resonant modes of uncoupled cavities and attributes the coupling between different cavities as the mechanism responsible, e.g., a weakly-transmitting mirror between two cavities or a small aperture in a commonly shared wall. The other approach views phase-locked modes as a result of a process that locks together the resonant modes of the entire array structure, i.e., supermodes. The coupling mechanism in this case is spatial overlapping of the supermodes' fields.

Most of the previous work on phase-locked cavities were based on the former view [10-12], which is pertinent only for weak coupling, i.e., when a small amount of power is exchanged between different cavities. Weak coupling assumption also justifies, to some extent, the cross-saturation term [of the gain] being left out in these analyses because the "leakage" power from the other cavities is weak. However, a device such as SHB array, cannot be categorized as being weakly-coupled in the former sense because of its configuration, and therefore, the second view adopted by [13] appears to be more appropriate in this case. This also means that the discussions on phase-locked arrays in previous Coupled High Power Waveguide Laser Research reports [1-3] are not quite applicable here.

Unfortunately, there are a few practical difficulties associated with Shakir and Chow's approach: (1) supermodes for the entire array - in the absence of gain - need to be determined in advance somehow; and (2) except in special cases, it is difficult to calculate the quantities necessary for phase-locking analysis, such as coupling coefficients and self- and cross-saturation coefficients. Determining the supermodes is fairly straightforward for structures such as cascaded planar resonators in which transverse variation of the field can be effectively ignored [12,13]. In most other cases, however, it presents a major problem.

One way to calculate the supermodes of a passive SHB array involves expanding the unknown supermode in terms of a complete set of waveguide modes EH_{m1} - assuming a single transverse mode in the y-direction - and solving for self-consistent, eigensolutions in a manner similar to that of Fox and Li [14]. Unlike the Fox and Li approach which dealt with open optical resonators, however, the roundtrip propagation would not [and cannot] be carried out in terms of a diffraction integral here. Rather, because we are dealing with a enclosed, guiding structure, the field would be propagated on a [waveguide] mode-by-mode basis except in instances where the modes become coupled together for some reason, in which case mode conversion matrices representing those interactions would be required. An initial seed vector representing the modal expansion of some arbitrary field distribution would be propagated back and forth sufficient

number of times until only the eigenvector with the largest eigenvalue, representing the dominant supermode with the lowest loss, remains. This procedure can be repeated - a la Gram-Schmidt process - to obtain the other supermodes and their roundtrip losses.

This approach has a certain drawback in that it is expected to expend a considerable amount of computational time. However, there is no way to solve for supermodes of a SHB array analytically. In fact, it can be shown that in general, a multimode [transverse modes] treatment is required to match the boundary conditions in a SHB array, even in an idealized case where the dividing walls are infinitely thin and the end mirrors are flush with the waveguide. Only in the event that the guide lengths differ by multiples of a half-wavelength, a closed-form steady-state solution exists for such a structure: such a solution possesses a uniform distribution across the array, with each guide having same amplitude [see the Appendix for the derivation].

Let us proceed with the eigenvector analysis. In mathematical terms, the supermode equation for a SHB array laser would look something like:

$$(D_a P_a C_a P_b D_b P_b C_b P_a)\, v = \lambda v \tag{3.6}$$

where

$v = [v_{11}\ v_{12} \cdots v_{21}\ v_{22} \cdots \cdots v_{N1}\ v_{N2} \cdots]^T$
= eigenvector representing a supermode; for example, the component v_{jk} would be the complex amplitude of the the k-th waveguide mode in the j-th guide in the expansion of a certain supermode [whose field distribution is specified at a common output plane],

λ = eigenvalue; supermode's roundtrip gain (loss) factor,

D_a = matrix describing the diffraction coupling plus the transmission loss at the output coupler end of the array,

D_b = matrix describing the diffraction coupling plus the absorption loss at the maximum reflector end of the array,

P_a = matrix accounting for the propagation of the field from the midsection of the array to the output coupler end of the array [By reciprocity, propagation along the same path from the opposite direction is also described by P_a],

P_b = matrix accounting for the propagation of the field from the midplane of the array to the maximum reflector end of the array [Again, the reciprocity holds],

C_a = matrix describing the rearranging of [waveguide] modes that takes place when the field encounters the staggered dividing aperture walls located at the output coupler end of the array,

C_b = matrix describing the rearranging of modes that takes place when the field encounters the dividing aperture walls located at the maximum reflector end of the array.

The matrix product $D_a P_a C_a P_b D_b P_b C_b P_a$ represents a roundtrip propagation of the field. In the context of our 37 cm laser, the D matrices are expected to have a narrow diagonal band due to weak coupling between different waveguide modes, especially between those of different waveguides, whereas the C matrices could have a band of appreciable width. The P matrices, by construction, are purely diagnoal, with the diagonal components' values determined by the guide lengths and the waveguide modes' complex propagation constants.

Because of massive computational requirements, and because we already know that EH_{21} mode is the main component of the dominant supermode, actual numerical simulations based on the above algorithm were not carried out in this program. However, expressions required to evaluate the matrix coefficients are either readily available in the literature [6-9] or easily derivable, and implementing the procedure outlined above should be fairly straightforward. For the simulation, it may be necessary to try a range of frequency values to come up with a valid solution: in the case of a single cavity, any error in the initial estimation of the resonant frequency may be compensated for at the end from the phase of the eigenvalue [15], but that is not possible in our case because more than one [different] cavity lengths are involved.

In principle, once the lowest-loss supermodes of the array are obtained, phase-locking analysis may be carried out to determine some key features of the locked array such as locking range and locked frequency. This analysis is more amenable to open, planar resonators than waveguide resonators because of the absence of transverse field variation in the former. Still, the results of the analysis ought to provide some valuable insight into how the prescribed locking characteristics and other properties of a phase-locked array are affected by factors such as cavity length variations and the length of the coupling region. Although it is beyond the scope of this report to carry out the actual analysis, the required steps will outlined below for reference purpose, with the special case of two-mode oscillation serving as an example. For an in-depth discussion of the topic, the readers should refer to [13].

Suppose we represent the field in the array by a superposition of its supermodes, i.e., resonant modes for the entire array, as follows:

$$E(x,y,z,t) = \{ \sum_k a_k(t)\exp[-j(\omega_k t+\phi_k)]U_k(x,y,z) + \text{c.c.} \}/2 \qquad (3.7)$$

where
a_k = amplitude of the k-th supermode component
ϕ_k = phase of the k-th " "
ω_k = nominal frequency of the k-th supermode
$U_k(x,y.z)$ = field distribution of the k-th supermode.

Then, by assuming that $a_k(t)$ and $\phi_k(t)$ vary slowly on the scale of $2\pi/\omega_k$, and expanding the polarization of the medium to the third order, the following equation of motion can be obtained for the complex field amplitude $A_k(t) \equiv a_k(t)\exp[-j\phi_k(t)]$ from above:

$$dA_k(t)/dt = j(\omega_k - \Omega_k + j\Gamma_k)A_k(t) + \sum_l M_{kl}A_l(t)\exp[j(\omega_k-\omega_l)t] + \sum_\mu\sum_\rho\sum_\sigma T_{k\mu\rho\sigma}E_\mu E_\rho^* E_\sigma \exp[-j(\omega_\mu - \omega_\rho + \omega_\sigma - \omega_k)t]$$

where (3.8)

Ω_k = resonant frequency of the k-th supermode
Γ_k = non-resonant loss of the k-th supermode
M_{kl} = coupling coefficient [between the l-th and k-th modes]
$T_{k\mu\rho\sigma}$ = saturation coefficient.

Expressions for M_{kl} and $T_{k\mu\rho\sigma}$ are given in [13]; the former basically depends on the spatial overlap of the two supermode fields - weighted by the population inversion density - whereas the latter is a function of the spatial correlation among the modes designated by k, μ, ρ, and σ, - also inversion density weighted. Though not shown explicitly, each of the coefficients includes a self-relating term, e.g., a self-coupling term or a self-saturation term, in addition to the cross terms. At this time, it is important to realize that the cross-coupling [and cross-saturation] occurs between different supermodes and not between different cavities per se as in [10-12]. Incidentally, since we are dealing with equations of motion, both M_{kl} and $T_{k\mu\rho\sigma}$ are in units of 1/sec; they are normalized with respect to the roundtrip time of the array.

Let us now take a special case. When there are only two oscillating supermodes, as may be the case when the rest of the modes fall outside the gain curve, the set of equations given by (3.8) reduce to the following set of normalized equations [upon having replaced ω_1 and ω_2 by ω]

$$\begin{aligned} d\tilde{a}_i/d\tau &= (\alpha_{ii}-\Gamma_i)\tilde{a}_i - (R_{iiii}\tilde{a}_i^2 + 2R_{iijj}\tilde{a}_j^2)G(\xi)\tilde{a}_i \\ &\quad + \alpha_{ij}(\cos\phi - \xi\sin\phi)\tilde{a}_j, \qquad i,j = 1,2 \\ d\phi_i/d\tau &= \omega - \Omega_i - \xi\alpha_{ij} + (R_{iiii}\tilde{a}_i^2 + 2R_{iijj}\tilde{a}_j^2)G(\xi) \\ &\quad - \alpha_{ij}(\sin\phi + \xi\cos\phi)\tilde{a}_j/\tilde{a}_i, \end{aligned} \tag{3.9}$$

where

$\phi \equiv \phi_1 - \phi_2$
α_{11}, α_{22} = unsaturated gain for each mode
α_{ij} = coupling term; $\alpha_{12} = \alpha_{21}$
R_{iiii}, R_{iijj} = self- and cross-saturation terms, respectively; $R_{1122} = R_{2211}$
$G(\xi)$ = frequency dependence of the gain curve
ξ = laser frequency detuning parameter = $(\omega_o - \omega)/\gamma$
ω_o = atomic line center frequency
ω = nominal frequency
[operating frequency when phase-locked]
γ = atomic dipole decay constant
= width of the gain curve
τ = normalized time variable = γt.

In the above, $\tilde{a}_1$ and $\tilde{a}_2$ are normalized versions of a_1 and a_2; α's, R's, and frequencies ω and Ω's are normalized with respect to γ.

When the array becomes phase-locked, a steady state is reached, i.e., a_1, a_2, ϕ_1, and ϕ_2 no longer change with time. Thus, when N formerly-oscillating supermodes are locked together, obtaining the phase-locked solution amounts to numerically solving a system of 2N nonlinear equations for 2N variables: N amplitude variables, N-1 phase variables [one of the N phases can be chosen arbitrarily], and the

operating frequency ω.

3.4 Application of the Theory

In the two preceeding sections, we examined the loss mechanisms in SHB arrays and a systematic approach to [understanding] phase-locked arrays in general. In this section, we shall try to provide some explanations for the experimental results submitted in Section 2 by making use of the findings in Sections 3.2 and 3.3, with particular emphasis on relationships among cavity length variations, mode mismatch loss, supermode distribution, and the output power.

As shown in Section 3.2, mode mismatch loss is a major component in the total loss, and it increases with severity of "misfit" between the fields in two neighboring guides. This misfit, i.e., deviation of the two collective fields from a pure EH_{21} mode, can occur as a result of either a deviation of the phase difference between the two from 180° or a disparity in their amplitudes. [It is true that the mode mismatch loss will not be zero even if the field in each of the two guides fits the EH_{21} mode perfectly because of the finite thickness of the dividing wall. Nevertheless, the mismatch loss is significantly higher when there are disparities between the two neighboring fields.]

A phase mismatch can be caused by any of several events: a tilt of the end mirrors, a change in the temperature distribution from one cavity to the next, or a nonuniform discharge density across the array, just to name a few. All these can contribute to a spread in "effective" cavity lengths and a phase mismatch between a pair of guides. On the other hand, an amplitude mismatch may be a result of uneven intracavity losses - the eight-element experiment with a ceramic piece in one of the guides is a good example of that - or perhaps a secondary effect due a phase mismatch. In a phase-locked array, effects of the two driving mechanisms behind mode mismatch loss tend to reinforce each other and cannot be easily separated. For instance, in the eight-element experiment with a lossy ceramic piece [cf. Section 2.2], in addition to the very unbalanced near field intensity distribution, we also observed pairwise far field patterns which indicated, on the average, much larger phase mismatches than in the no-ceramic case.

Perhaps, the most important consequence of increased mode mismatch loss is a reduction in output power, and there are convincing evidences that phase mismatches do lead to a power reduction. This can be seen in several experiments, of which the most convincing is the output power vs. tilt measurements; in the two-, eight-, and ten-element experiments, the output power dropped off sharply with increasing amount of mirror tilt. Considering that the PZT's are capable of displacing mirrors by only a few μm's, their effect on the end mirror coupling losses should be minimal. It is also quite unlikely that the mode composition of the dominant phase-locked array mode would be changed by a tilt of such magnitude to the point where the net propagation losses of the mode are significantly affected. It must then be concluded that the mode mismatch loss induced by phase mismatches in the array is probably the underlying mechanism

responsible for the sharp decrease in output power. We now offer more substantive arguments.

First, we shall illustrate the close connection that exists between the phase profile of a locked-array and the profile of the effective cavity length. To that end, we tried to guess what the phase profile of an actual field distribution might be like by using the pairwise far field scans from the eight-element SHB array experiment [cf. Figure 2-5]. This involved estimating the phase mismatches from the pairwise farfield patterns by comparing them to computer-generated plots of far field patterns for two EH_{21} lobes of different phases and amplitudes. The result is that the phase mismatch was decidedly larger with the end elements, with the estimate in the 30°- 45° range. In the middle portion of the array, the mismatch was close to zero. Phase mismatch estimates of Figure 2-5 are, from left to right, 45°, 30°, 0°, 0°, 10°, 30°, and 35°, respectively. These findings, and the fact that the pairwise far field patterns are quite symmetric with respect to the center of the array, are consistent with our knowledge of a typical effective cavity length profile. Measurements reported in the previous reports and in earlier sections of this report, e.g., the beat frequency measurements, strongly suggest that the index profile of the array is mostly flat except in the vicinity of the end elements, where the index shows a sharp increase, probably because the cooling is most efficient in those regions. Thus, we are led to believe that there is a close correlation between the phase profile and the effective cavity length profile of a phase-locked array.

Tilting the coupler mirror, via the tilt PZT, introduces a linear variation to the effective cavity lengths across the array. [In fact, it introduces a linear variation within each element as well, but for now, consider the effective cavity length within each guide as being constant.] If we crudely assume, for simplicity sake, that the index variation across the array has a parabolic profile, it can be shown that a modest amount of tilt can lead to a larger effective cavity length variation on the average compared to the no-tilt case. [Of course, the effective cavity length profile will be no longer symmetric then]

Having established that a modest tilt of the end mirror can lead to a substantial amount of effective cavity length variations and a significant phase mismatch between the fields in adjacent elements, and having dismissed the possibility of the propagation loss playing a major role, we can safely attribute the lower output power in the presence of a tilt to an increased mode mismatch loss [due to larger phase mismatches]. Let us now apply a similar type of reasoning to explain other important features of phase-locked SHB arrays.

One key feature which mode mismatch loss mechanism may help explain concerns the array's intensity profile. In an uncoupled array, without the mode mismatch loss, the roundtrip loss is very similar for all elements, this being reflected in its rather uniform, top-hat-like near field scan. The SHB array, on the other hand, is very susceptible to having an uneven loss distribution, with the elements near each end usually suffering the largest mismatch loss because of their steep index changes. A proof of that shows up in its intensity profile which tapers off away from the center. When a tilt is applied, the phase mismatch

becomes greater on one side and smaller on the other side - because of the nonuniform but symmetric index profile which exists in the first place - with corresponding changes in the loss profile. As a result, the peak of the intensity profile is shifted toward the end where the tilt has brought the mirror closer to the waveguide.

We believe that mode mismatch loss is also responsible for vastly inferior power output of phase-locked SHB arrays in comparison with uncoupled arrays. For example, at 90 torr and 1100 W of rf power, the maximum output power was measured at 41 and 68 W for the ten-element SHB array and the uncoupled ten-element array, respectively [cf. Tables 2-4 and 2-5]. There are two reasons for our conjecture: (1) Unlike the SHB array, the uncoupled structure does not have mode mismatch losses; and (2) With a locked SHB array, nonuniform physical characteristics such as effective cavity length variations only add to the mode mismatch and propagation losses. Because of these inherent discrepancies, uncoupled arrays are guaranteed to enjoy a superior output power. [Of course, the difference can be made smaller].

For further evidences in support of these claims, we can look to the results from the portion of the two-element array experiment in which the effects of various degrees of tilt were monitored. Even though the array has a slightly different structure from the eight- and ten-element SHB arrays, it, nevertheless, is quite similar to them in character, and the features we have been discussing in the framework of the SHB arrays are beautifully demonstrated in Figures 2-11 and 2-12.

As a good measure, output power for the eight-element SHB array was predicted with our model - calculated using a simple Rigrod program - and compared to the experimental value. At 80 torr of pressure and 1000 W of input power, the measured value was in the range of 45-50 W. The predicted value, on the other hand, was about 43 W. For the theoretical prediction, expected power output was computed for each guide individually and then summed up, since the losses varied from guide to guide [for mode mismatch loss calculations, the phase mismatch estimates from Figure 2.5 were used]. The agreement between the two numbers is fairly good, considering that our estimate was based on several approximations. [We had originally hoped to use the ten-element array data; however, because of the frequent occurence of the uneven discharge problem and the possibility of some laser misalignment during the measurement process, we opted to use the result of the eight-element array experiment which went much more smoothly]

Also, recall from Section 2.3 that the output power of the two-element array had decreased with increasing coupling length. This, too, makes sense in view of the fact that a longer coupling region would allow the composite field from the two guides to smear out more into the central region of the array and thus would lead to a larger mode mismatch loss.

Finally, we would like to discuss another interesting result from the two-element experiment, namely the relationship between the locking range and pressure. We had reported that the locking range increased with pressure. Although it is well known that an increase in pressure

increases the saturation intensity [16], which, in a relative sense, implies diminished gain saturation [for a fixed intensity level], it is not clear at this time what effect reduced gain saturation would have on the locking range, nor has it been discussed in the literature to our knowledge. It may also be possible that an increase in the width of the gain curve and the small-signal gain that accompanies an increase in pressure play a more critical role than the increased saturation intensity. Perhaps, the coupled equations of motion (3.9) could be solved for various parameter values reflecting the changes in the cavity pressure; then, perhaps, we could look for a possible connection.

4.0 DISCUSSIONS

4.1 Summary

By focussing on the effects of a PZT tilt on the output power, array intensity distribution and pairwise farfield patterns, we have deduced that the effective cavity length variations are responsible for many of the observed features of phase-locked SHB arrays and also for the discrepancies in the behavior of an uncoupled array and a SHB array. Among the several loss mechanisms investigated, mode mismatch loss was identified as the primary mechanism through which the effective cavity length variations manifest themselves.

During the course of the experiments, some unexpected events were encountered. One of them was the appearance of uneven discharge distribution, especially at low input power and high pressure values. The other was the finding that one very lossy element can effectively shut down the entire array; we did expect a rippling effect on the neighboring elements because all the elements are locked together, but the extent to which they were affected was a surprise.

4.2 Future Work

There are several things that can be done to further improve our understanding of phase-locked arrays, especially SHB arrays, and their performances. They are outlined below.

On the theoretical side, the following items could be looked at. One, we need to learn more about the locking properties of arrays in general. For example, how are the locking ranges and phase-locked frequencies determined? How are they related to the individual cavities' resonant frequencies? And so forth. The formulation outlined in Section 3.3 could be used to answer some of these questions. Two, supermodes of a passive array need to be calculated more accurately so that more precise estimates of the losses and the output power can be made. With sufficient computation capability, the eigenvalue approach detailed in Section 3.3 should give fruitful results. Three, a parametric study on the mode mismatch loss needs to be done. Finding out optimal values of the guide dimensions - recall that the mismatch loss is especially sensitive to the guide widths - could potentially reduce the loss dramatically. Four, a [numerical] thermal analysis of the array can be done to accurately estimate the temperature distribution across the array. How does the distribution change as we increase the number of elements in the array? Obviously, it would be disastrous if the temperature profile, and thus the index profile, continued to become more nonuniform. However, we suspect that the temperature gradient to remain steep only near the outer few elements regardless of the array size. Five, the results of this program could be generalized to SHB arrays with round guides. In principle, the underlying mechanisms controlling their behavior should be no different

from those of the square guide arrays. We just need to take into account the specific differences arising from the difference in geometry.

On the experimental side, items that should be looked at are as follows. One, we need more detailed measurements of the index profile in an uncoupled array [although measurements with a SHB array would be preferrable, that seems quite difficult]. This could be done by taking the output from a pair of elements at a time and measuring the beat frequencies. Two, it would be useful to implement a means of controlling the effective cavity lengths individually so that the array can be made more "uniform," thereby minimizing the phase mismatches. One crude and less ambitious way to counter the effect of uneven cooling might be to replace the flat maximum reflector mirror with a slightly convex mirror. Three, we may want to consider designing a new type of amplitude modulator by utilizing the dramatic effect that a large loss in just one element can have on the output power of the entire array. One possible such setup would be to replace the maximum reflector mirror with a partially transmitting mirror; the field would be coupled out to an external cavity, where [amplitude of] the field would be spatially modulated, perhaps by a small electrooptic modulation cell in the middle, and then coupled back into the waveguide [see Figure 4-1]. This modulation technique would produce a faster response compared to a direct modulation of the rf excitation itself, and also would be fairly economical in terms of power consumption and size. Four, it would be intersting to see how dramatic the effect of changing the wall thickness and guide width would be on the performance of SHB arrays. It seems clear enough that one way to minimize the power loss in a phase-locked SHB array would be to decrease the wall thickness. [This point was unequivocally demonstrated in pp.3-17 and 3-18 of [3]]. An interesting question to ask may be "how small can the wall thickness be made without seriously affecting its ability to confine the field within the guide and at the same time extract heat efficiently?" In the limit when the wall thickness goes to zero - thus the mode mismatch loss - does the output power approach the value of an uncoupled array? And how does a guide optimized for minimum mode mismatch loss fare in other respects, such as gain per unit length and propagation loss? Finally, we need to examine the issue of nonuniform discharge distribution, which obviously cannot be tolerated for array applications.

Perhaps the most worthwhile experiment to perform based on the items listed above would be to build a SHB array laser with very thin dividing walls and individually [length-] tunable guides. It would be interesting to see whether such a device could indeed behave as a low-loss laser with a uniform intensity profile as predicted by theory.

Figure 4-1 A Schematic Diagram of a Potential Amplitude Modulator for Phase-Locked Arrays

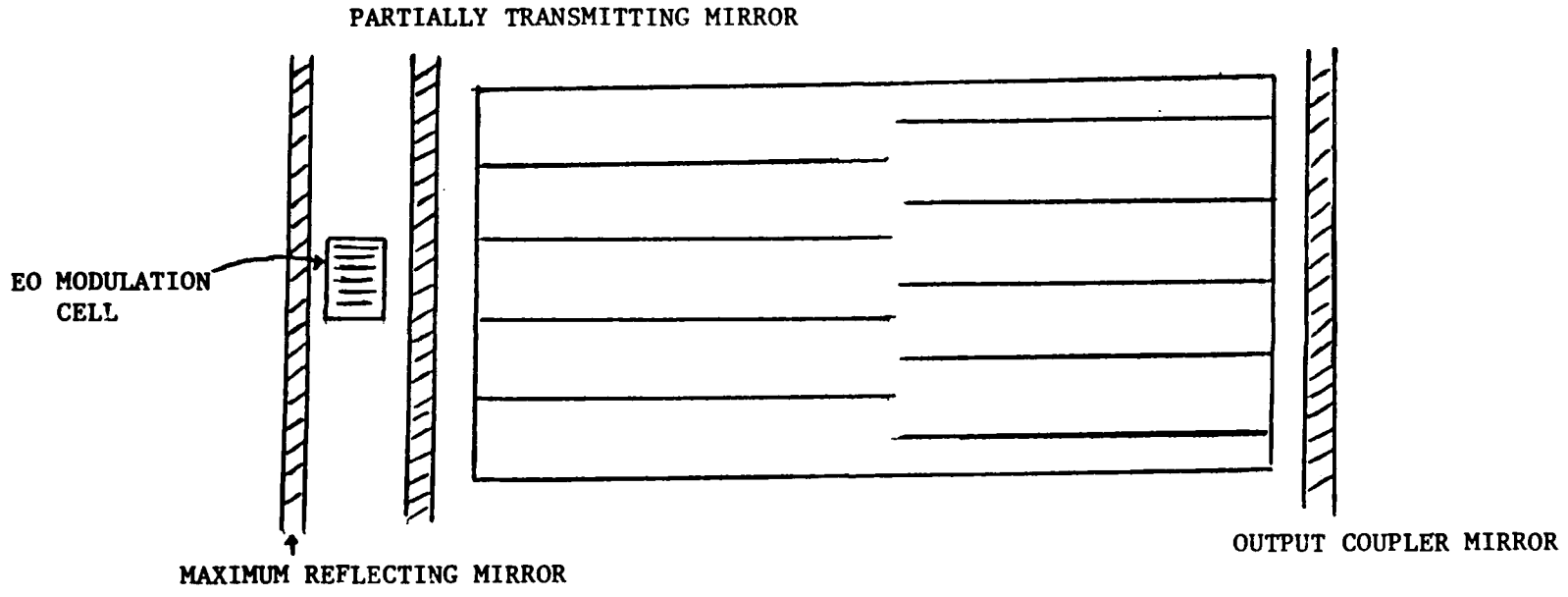

APPENDIX

Here, we shall show that the dominant supermode for an idealized SHB array structure - having infinitesimally thin dividing walls and effective cavity lengths that differ by multiples of a half-wavelength - has a uniform profile across the array and consists of only EH_{21} waveguide mode.

Assume that the electric field in the m-th guide is given by the EH_{21} waveguide mode as follows:

$$E_m(x,y,z) = \hat{x}\,\{E_{m+}\exp[-j\beta z] + E_{m-}\exp[+j\beta z]\}\sin(2m\pi(x-x_m)/a) \cdot\sin(m\pi(y-y_m)/b) \tag{A.1}$$

where

E_{m+}, E_{m-} = complex amplitudes of the counterpropagating waves
β = propagation constant of the EH_{21} mode
x_m, y_m = the coordinates of the center of the m-th guide
a, b = guide dimensions.

E_{m+} and E_{m-} are related by

$$E_{m+} = RE_{m-}\exp[2j\beta l_m] \tag{A.2}$$

where

l_m = the effective cavity length of the m-th guide
R^m = the end mirror's reflection coefficient.

If we further assume a perfectly reflecting mirror at each end for convenience, Eqn. (A.1) can be cast in the form of

$$E_m(x,y,z) = \hat{x}\,A_m\sin(\beta(z-l_m))\sin(2m\pi(x-x_m)/a)\cdot\sin(m\pi(y-y_m)/b) \tag{A.3}$$

with the corresponding [approximate] magnetic field expression being given by

$$H_m(x,y,z) = \hat{y}\,j(A_m/\eta_o)\cos(\beta(z-l_m))\sin(2m\pi(x-x_m)/a)\cdot\sin(m\pi(y-y_m)/b) \tag{A.4}$$

where η_o is the characteristic impedance of the medium. As usual, the other field components, which are orders of magnitude smaller, have been left out [7].

Next, we try to match the boundary conditions at $z = 0$, i.e., at the plane where the two staggered sections of the array meet. In a SHB array, the fields from two neighboring guides couple into one guide [except with the end elements]. Suppose we label the two neighboring guides the m-th and the (m+2)th guide, and the guide they are butted up against the (m+1)th guide.

The boundary conditions consist of matching $E_m(x,y,0)$, $H_m(x,y,0)$ with $E_{m+1}(x,y,0)$, $H_{m+1}(x,y,0)$, and $E_{m+2}(x,y,0)$, $H_{m+2}(x,y,0)$ with $E^m_{m+1}(x,y,0)$, $H^m_{m+1}(x,y,0)$, respectively, in the appropriate regions of x. Because we are working under the assumption of only the EH_{21} mode existing in the array, the two sets of boundary conditions in turn require that $E_m(x,y,0)$ and $H_m(x,y,0)$ be replicas of $E_{m+2}(x,y,0)$ and $H_{m+2}(x,y,0)$, respectively.

Thus, we have the following relations.

$$\begin{aligned} & A_m \sin(\beta l_m) = A_{m+2} \sin(\beta l_{m+2}) = -A_{m+1} \sin(\beta l_{m+1}), \\ \text{and} \quad & A_m \cos(\beta l_m) = A_{m+2} \cos(\beta l_{m+2}) = A_{m+1} \cos(\beta l_{m+1}). \end{aligned} \tag{A.5}$$

For these relations to be satisfied simultaneously, the following must hold true:

$$\begin{aligned} & \beta(l_m - l_{m+2}) = n\pi, \qquad n = 0,1,2,\ldots \\ & \beta(l_m + l_{m+1}) = p\pi, \qquad p = 0,1,2,\ldots \\ \text{and} \quad & \beta(l_{m+2} + l_{m+1}) = q\pi, \qquad q = 0,1,2,\ldots \end{aligned} \tag{A.6}$$

Obviously, same type of relationships must prevail with other guides of the array as well. What do these conditions imply? The first condition above states that the length of the guides in each of the array's two staggered sections must differ by multiples of a half wavelength. The second and third conditions, on the other hand, state that the combined guide length of the two sections must add up to multiples of a half wavelength, which also happens to be the condition required for oscillation in a single-cavity laser.

It is clear that when the above conditions are met, the field distribution at any arbitrary plane across the array would be a periodic repetition of the EH_{21} profile, with equal amplitude in each guide.

REFERENCES

1. Newman, L.A., A.J. Cantor, W.J. Fader, R.A. Hart, J.T. Kennedy, and A.J. DeMaria, "Coupled High Power Waveguide Laser Research," Final Technical Report under Contract No. F49620-84-C-0062, July 30, 1985.

2. Cantor, A.J., R.A. Hart, J.T. Kennedy, and L.A. Newman, "Coupled High Power Waveguide Laser Research," Interim Technical Report under Contract No. F49620-85-C-0106, October 31, 1986.

3. Cantor, A.J., R.A. Hart, J.T. Kennedy, and L.A. Newman, "Coupled High Power Waveguide Laser Research," Final Report under Contract No. F49620-85-C-0106, September 1987.

4. Newman, L.A., R.A. Hart, J.T. Kennedy, A.J. Cantor, A.J. Demaria, and W.B. Bridges, "High Power Coupled CO_2 Waveguide Laser Array," Applied Physics Letters, Vol. 48, No. 25, p. 1701, June 23, 1986.

5. Hart, R.A., L.A.Newman, A.J.Cantor, and J.T.Kennedy, "Staggered Hollow-bore CO_2 Waveguide Laser Array," Applied Physics Letters, Vol. 51, No: 14, pp. 1057-1059, October 1987.

6. Hill, C.A. and D.R. Hall, "Waveguide Laser Resonators with a Tilted Mirror," IEEE Journal of Quantum Electronics, Vol. QE-22, No. 7, pp. 1078-1087, July 1986.

7. Laakman, K.D. and W.H. Steier, "Waveguides: Characteristic Modes of Hollow Rectangular Dielectric Waveguides," Applied Optics, Vol. 15, No. 5, pp. 1334-1340, May 1976.

8. Bounois, J. and G.P. Agraval, "Mode Discrimination and Coupling Losses in Rectangular Waveguide Resonators with Conventional and Phase-conjugate Mirrors," Journal of Optical Society of America, Vol. 72, No. 7, pp. 853-860, July 1982.

9. Abrams, R.L., "Coupling Losses in Hollow Waveguide Laser Resonators," IEEE Journal of Quan. Electronics, Vol. QE-88, No. 11, pp. 838-843, November 1972.

10. Spencer, M.B. and W.E. Lamb, Jr., "Theory of Two Coupled Lasers," Physical Review A, Vol. 5, No. 2, pp. 893-898, February, 1972.

11. Fader, W.J., "Theory of Two Coupled Lasers," IEEE Journal of Quantum Electronics, Vol. QE-21, No. 11, pp. 1838-1844, November 1985.

12. Mirels, H., "Saturation Effects in Coupled Lasers with Homogeneous Gain," Applied Optics, Vol. 26, No. 1, pp. 47-51, January 1987.

13. Shakir, S.A. and W.W. Chow, "Semiclassical Theory of Coupled Lasers," Physical Review A, Vol. 32, No. 2, pp. 983-991, Augst 1985.

14. Fox, A.G. and T. Li, "Computation of Optical Resonator Modes by the

Method of Resonance Excitation," IEEE Journal of Quantum Electronics, Vol. QE-4, pp. 460-465, July 1968.

15. Siegman, A.E., Lasers, Chs. 24 and 29, University Science Books, Mill Valley, Calif., 1986.

16. Yariv, A., Introduction to Optical Electronics, 2nd Ed., pp. 191-193, Holt, Rinehart and Winston, New York, 1976.